

Spectrin Binding of the Antileukemia Drug, Imatinib Mesylate

a project by

Uttam Pal

Department of Biophysics
University of Calcutta



under the guidance of

Professor Abhijit Chakrabarti

Structural Genomics Section, Biophysics Division
Saha Institute of Nuclear Physics, Kolkata



18 May to 31 July 2009

Contents

Preface.....	iii
Acknowledgements.....	iii
Certificate from the Supervisor.....	iv
Synopsis	5
Section I: Study of the interaction between Imatinib and Erythroid Spectrin	
1. Background.....	6
2. Materials and Method.....	8
3. Results	10
4. Discussion	13
5. References.....	15
Section II: Understanding UV-Visible Spectroscopy	
1. Light Absorption & Excitation	20
2. Study of Absorption Spectroscopy.....	22
3. Relaxation of Excited State molecules	25
4. Study of Fluorescence Spectroscopy.....	27
5. Instrumentation	33
6. Appendix.....	35
7. References	38
Section III: Understanding CD Spectroscopy	
1. Introduction.....	40
2. Results and Discussion	42
3. References.....	44
End Note	45

Preface

The project entitled 'Spectrin Binding of the Antileukemia Drug, Imatinib Mesylate' was carried out during the period of 18 May to 31 July 2009, under the supervision of Professor Abhijit Chakrabarti, Structural Genomics Section, Biophysics Division, Saha Institute of Nuclear Physics, Kolkata, as a part of the M. Sc. Biophysics part II syllabus of University of Calcutta. The tenure was organized by Centre for Advanced Research and Education (CARE), Saha Institute of Nuclear Physics, Kolkata.

Acknowledgements

I would like to convey my sincere thanks to Professor Abhijit Chakrabarti for his guidance throughout my training period to Professor Samita Basu for helping me to understand UV-Visible Spectroscopy from the very base to the very core, which was the major tool used in my project work. I am grateful to Professor Pradeep Kumar Sengupta for teaching me the basics of CD spectroscopy. I express my gratitude to Mousumi Banerjee for her continuous help and dedication.

I thank my lab-mates Pradipto Samanta, Sourav Maiti, Ipsita Kundu and Manish Banerjee for their involvement in the project gave it a feel of a group work. I thank research scholars Sumanta Basu, Madhumita Chakraborty and Avik Basu of Biophysics Division; and Brotati Chakraborty and Manas Kumar Sarangi of Chemical Science Division for their valuable advices. I heartily thank *everyone else* concerned directly or indirectly with the fulfillment of this project.

I thank Centre for Advanced Research and Education, SINP for selecting me as a summer trainee, for the laboratory facilities provided, and for the interactive session organized. I also thank Structural Genomics Section, Biophysics Division and Chemical Science Division, SINP where I have conducted many of my experiments.

Finally, I would like to thank Department of Biophysics, University of Calcutta for the implementation of summer project as a part of our syllabus, and Saha Institute of Nuclear Physics, Kolkata as a whole for the hospitality received.

Uttam Pal

Kolkata, India
27 July 2009



साहा इंस्टिट्यूट ऑफ न्यूक्लियर फिज़िक्स
SAHA INSTITUTE OF NUCLEAR PHYSICS

सेक्टर-I, ब्लॉक 'ए.एफ', बिधाननगर / SECTOR-I, BLOCK-'AF', BIDHANNAGAR

कोलकाता-700 064, (भारत) / KOLKATA-700 064, INDIA

ग्राम / GRAM : 'NUCLISTUTE' KOLKATA

दूरभाष / PHONE : 2337-5345-49 (5 LINES), फैक्स / FAX : 0091-33-2337-4637

To Whom It May Concern

This is to certify that Mr. Uttam Pal, final year student of Biophysics, Molecular Biology & Bioinformatics, University of Calcutta has worked in my laboratory during the month of mid May till end July, 2009 in the project entitled "*Spectrin Binding of the Antileukemia Drug, Imatinib Mesylate*" under my supervision.

Abhijit Chakrabarti

Professor

Biophysics Division & Structural Genomics Section

Saha Institute of Nuclear Physics, Kolkata

Synopsis

Section I: Study of the interaction between Imatinib and Erythroid Spectrin

Imatinib represents the first in the class of drugs targeted against chronic myelogenous leukemia to enter the clinic, showing excellent efficacy and specificity for bcr-abl, c-Kit, PDGFR kinases. But, it is not devoid of any hazards, one being hemolytic anemia. Recent screens are being carried out to find off-target proteins that bind to imatinib. This study looks for whether the drug has any effect on the major membrane cytoskeletal protein of the red blood cells, spectrin.

In this study imatinib mesilate has been shown to bind the erythroid membrane cytoskeletal protein spectrin with a binding dissociation constant of $5.8 \times 10^{-5} M$ at 25°C, which is comparable to the binding constant of imatinib with human serum albumin (HSA). Imatinib binding parameters has also been compared with that of other hydrophobic ligands to erythroid spectrin. Binding was detected by monitoring the quenching of tryptophan fluorescence intensity with the increasing concentrations of imatinib. The thermodynamic parameters associated with the binding indicated the interaction between imatinib and spectrin to be enthalpy-driven and partial immobilization due to hydrophobic association leading to the van der Waals or H-bonding type of interaction is likely to be the mechanism of binding. Binding stoichiometry of about 120 indicates that the binding occurs to the hydrophobic patches along the worm like spectrin molecule. Molecular docking study with a model spectrin repeat unit from Protein Data Bank also supported the experimentally obtained data.

Section II & III: Understanding UV-Visible & CD Spectroscopy

In these sections UV-Visible and CD spectroscopy, which had been the major tools for the study of spectrin imatinib interaction, has been reviewed. Absorption experiments were carried out with anthracene as a standard sample. Absorption of spectrin and imatinib has also been studied. Fluorescence quenching study of anthracene with N,N-dimethylaniline was performed. Some associated phenomena like Stokes' shift, mirror image rule of absorption and emission have been shown. CD spectra of spectrin, which has the α helix as its major constituent were obtained and commented.

Background

Imatinib mesilate (STI-571, Gleevec) is a selective tyrosine kinase inhibitor [1], successfully used for the treatment of chronic myelogenous leukaemia (CML) and gastrointestinal stromal tumors [2]. The drug partly occupies the ATP-binding pocket and stabilizes an inactive form of the Bcr-Abl oncogenic fusion protein [3]. However, it can also target other proteins not involved in causing malignancies [4, 5]. CML is caused by expression of a single oncoprotein resulting from the fusion of the BCR and ABL genes [6]. The Abl protein is a ubiquitously-expressed tyrosine kinase involved in multiple signaling pathways, and the fusion of the Bcr protein to the N-terminus of Abl in hematopoietic stem cells results in an oncoprotein with unregulated tyrosine kinase activity [7]. This causes cell proliferation, ultimately leading to leukemic transformation [8]. Imatinib, a 2-phenylaminopyrimidine compound (Figure 1-1) that represents the first in a class of targeted anticancer drugs developed to treat CML through inhibition of Bcr-Abl [9]. Imatinib is remarkably specific, and is effective against a very limited set of tyrosine kinases, including Kit, PDGFR and DDR in addition to Abl [10]. Imatinib inhibits Abl specifically by binding to an inactive kinase domain conformation that is characteristic of Abl [3, 11, 12].

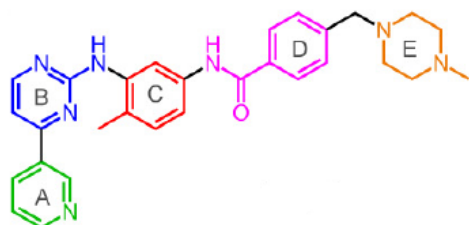


Figure 1-1: Imatinib (STI-571), consists of a pyridine ring (A, green), an aminopyrimidine ring (B, blue), a methylbenzene ring (C, red), a benzamide ring (D, magenta), and a N-methylpiperazine ring (E, orange).

Spectrin is a long, thin, flexible rod like protein about 100 nm in length that constitute around 25% of membrane associated protein mass of red blood cell. It is a heterodimer, consists of two antiparallel, loosely intertwined, flexible polypeptide chains (Figure 1-2) called α (280 kDa) and β (246 kDa) [13]. These are attached noncovalently to each other at multiple points, including both ends. Both the α and the β chains are composed largely of 106 amino acids long repeating domains [14].

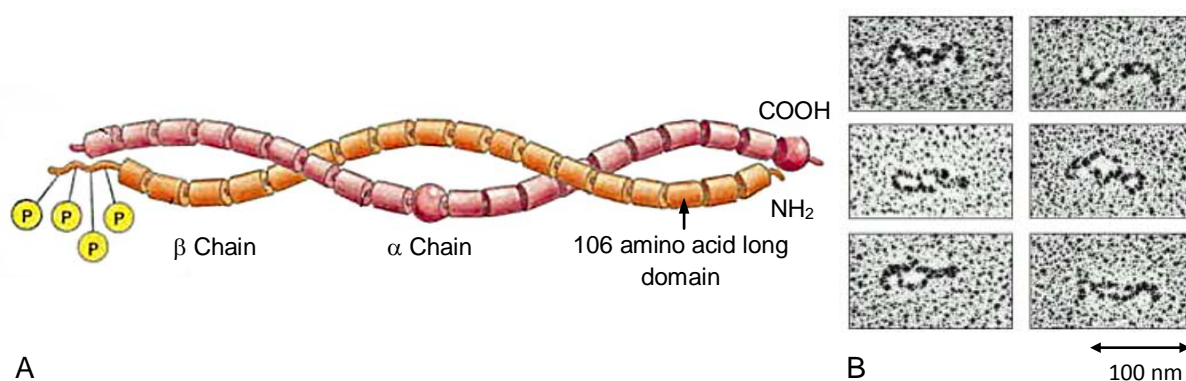


Figure 1-2: Spectrin molecule from human red blood cells. The protein is shown (A) schematically [14] and (B) in electron micrographs [15]. Phosphorylated 'head' end is on the left.

The spectrin heterodimers self-associate head-to-head to form 200 nm long tetramers. The tail ends of four or five tetramers are linked together by binding to short actin filaments and to other proteins such as adducin, band 4.1 in a junctional complex. The final result is a deformable, netlike meshwork

that underlies the entire cytosolic surface of the membrane (Figure 1-3), maintaining the structural integrity and biconcave shape of this membrane. It is this spectrin-based cytoskeleton that enables the red cell to withstand the stress on its membrane as it is forced through narrow capillaries. Genetic abnormalities in spectrin are associated with spherical and fragile red cells and hemolytic anemia [13].

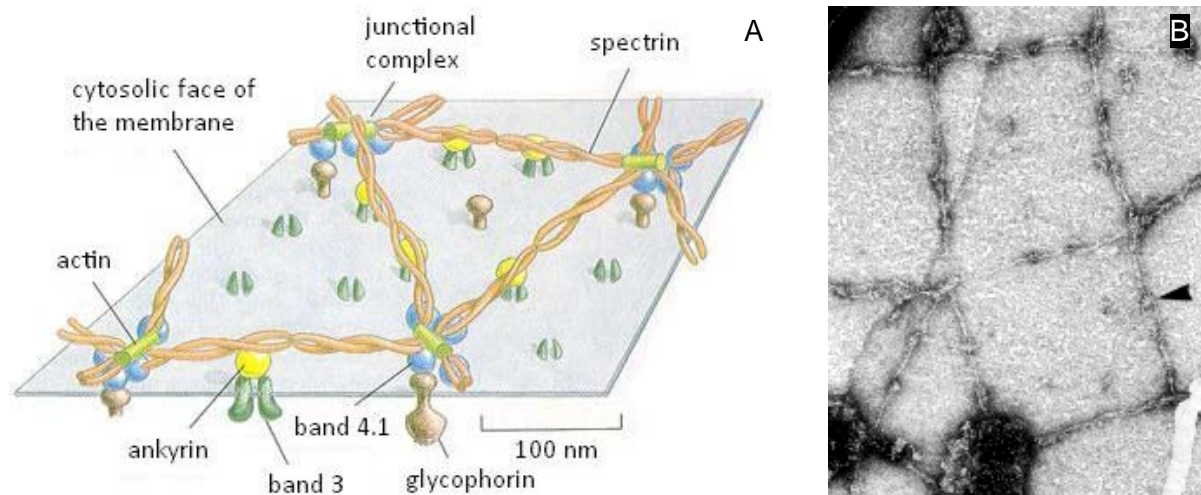


Figure 1-3: The spectrin based cytoskeleton on the cytosolic side of the human red blood cell membrane. The structure is shown (A) schematically [13] and (B) in an electron micrograph [16].

Daily doses of imatinib vary from 300 mg to 800 mg [17]. It is administered orally and its bioavailability *i.e.* percent of administered drug reaching systemic circulation is very high, about 98% [17]. It may not be “the magic bullet” and there may be alternative targets till undiscovered. Many side effects has been reported and one of them being hemolytic anemia. Spectrin has been shown to bind ATP [18] and the drug also binds to the ATP binding site of the two protein kinases [3, 11, 12]. In blood, both the red and white blood cells get equally exposed to the drug. After passing through the bilayer of red blood cells, the first thing imatinib will encounter is the spectrin-based cytoskeleton beneath the membrane. Will it bind to it? This is the first question whose answer we searched for.

Materials and methods

Imatinib mesylate/mesilate (Veenat) purchased from Natco Pharma. Tris, phenylmethylsulfonyl fluoride (PMSF), dithiothreitol (DTT), and EDTA were purchased from Sigma (St. Louis, MO, USA). Sodium dihydrogen phosphate and disodium hydrogen phosphate were purchased from Merck, Germany. Deionized water, twice distilled on quartz, was used for preparing solutions and buffers. Stock solution of imatinib was prepared in phosphate buffer and its concentration was determined by absorbance measurement on a Varian Cary 50 spectrophotometer, using a molar extinction coefficient of $32500\text{ M}^{-1}\text{ cm}^{-1}$ at 255 nm [19] and a 1 cm pathlength quartz cuvette.

White ghosts from goat blood were prepared by hypotonic lysis in 5 mM phosphate, 1mM EDTA containing 20 $\mu\text{g/ml}$ PMSF at pH 8.0 and spectrin dimers were purified following published protocols [20, 21, 22]. Spectrin extraction was done by resuspending the erythrocyte ghosts in 20 volume of spectrin removal buffer (0.2 mM sodium phosphate, 0.1 mM EDTA, 0.2 mM DTT, 20 $\mu\text{g/ml}$ PMSF, pH 8.0), and incubating at 37°C for 30 min. The crude spectrin was collected in the supernatant after centrifugation and was purified after concentration by 30% ammonium sulfate precipitation according to the method of Gratzer [20]. Spectrin was stored in the buffer containing 5 mM phosphate, 20 mM KCl, 1 mM EDTA, pH 8.0 containing 0.2 mM DTT. The protein was dialyzed extensively against the buffer containing 10 mM Na_2HPO_4 , 50 mM KCl, pH 7.4 to remove DTT before all fluorescence experiments. The purity of the preparation was checked by 7.5% SDS-PAGE under reducing conditions. The purified protein showed the characteristic spectrin dimer (α -chain of apparent molecular mass of ~ 240 kDa and β -chain of ~ 220 kDa) upon staining the gel with Coomassie blue. Spectrin concentrations were determined spectrophotometrically from an absorbance of 10.7 at 280 nm for 1% spectrin solution [20]. Absorbance at 280 nm was hemoglobin corrected using the following equation [20]:

$$OD_{280}^{corr} = OD_{280}^{obs} - 1.25 \cdot OD_{345}^{obs} \quad (1)$$

Fluorescence measurements

Steady-state fluorescence was measured in a Varian Cary Eclipse spectrofluorimeter using a 1cm pathlength quartz cuvette. The buffer used in the present study contained 10 mM Na_2HPO_4 , 50 mM KCl, pH 7.4. Small aliquots of an aqueous stock solution of imatinib mesylate were added to 0.1 μM spectrin for fluorescence measurements using excitation at 295 nm and slits with bandpasses of 5 nm for excitation and 10 nm for emission channels. Spectrin-free buffer containing different concentrations of imatinib was used as reference blanks in all fluorescence measurements. Fluorescence intensities were corrected for the inner filter effect due to absorption of the spectrin and imatinib, when absorbance, at both excitation and emission wavelengths, of the samples exceeded 0.05 [23]. All measurements were performed at 25°C, unless otherwise mentioned, with multiple sets (three to five) of samples.

Evaluation of binding constants

Any change in the fluorescence emission intensity of spectrin ($\lambda_{ex} = 295\text{ nm}$, $\lambda_{em} = 340\text{ nm}$) upon the progressive addition of imatinib was measured to evaluate the binding constant. Results from fluorescence titrations were analyzed by the following methods. Apparent dissociation constant

($K_d = 1/K_{app}$) was determined using double reciprocal curve analysis (Equations 2) based on the following equilibrium:

$$STI + Sp = [STI - Sp]$$

Where STI represents Imatinib mesylate (STI-571) and Sp represents spectrin. All experimental points for binding isotherms were plotted by least-square analysis. A double reciprocal plot was drawn using:

$$\frac{1}{\Delta F} = \frac{1}{\Delta F_{max}} + \frac{K_d}{\Delta F_{max}} \cdot \frac{1}{C_d} \quad (2)$$

ΔF is the change in fluorescence emission intensity at 340 nm ($\lambda_{ex} = 295 \text{ nm}$) for each point of the titration curve, ΔF_{max} is the same parameter when the ligand is totally bound to spectrin, C_d is the concentration of drug, and K_d is the apparent dissociation constant.

The approach is based on the assumption that emission intensity is proportional to the concentration of the ligand and $C_d \gg C_s$ i.e. when ligand concentration is in large excess over the spectrin concentration. An estimate of the stoichiometry of imatinib binding to spectrin was obtained from the intersection of two straight lines obtained from the least-square fit plot of normalized increase in fluorescence intensity against the ratio of input concentrations of imatinib and spectrin.

Evaluation of thermodynamic parameters

Thermodynamic parameters, ΔG (free energy), ΔH (heat content) and ΔS (entropy) were evaluated from the following equations:

$$\ln K_{app} = -(\Delta H/RT) + (\Delta S/R) \quad (3)$$

$$\Delta G = \Delta H - T\Delta S \quad (4)$$

Where R and T represents the universal gas constant and absolute temperature, respectively. The apparent binding constant ($K_{app} = 1/K_d$) was measured at five different temperatures to evaluate ΔH and ΔS from the slope and the intercept in a plot of $\ln K_{app}$ against $1/T$.

Molecular Docking study

NMR solution structure of the 16th repetitive motif of chicken brain α -spectrin (1AJ3) was obtained from Protein Data Bank and used as the model structure [24] for the molecular docking experiment. The structure of imatinib (STI_ideal) was also obtained from Protein Data Bank. The molecular docking was performed on Docking Server [25], which uses Autodock 4.0 for docking calculations and MOPAC 2007 for calculating semiempirical charges and geometry optimization on the ligands. The server optimizes the ligand geometry, calculates pH-dependent partial charges (pH was set to 7.4), and identifies rotatable bonds. It calculates electrostatic properties of the protein of interest and defines the ligand-binding region. The ligand-protein interaction is then calculated by a scoring function that includes terms and equations that describe the intermolecular energies. The result of a docking calculation is a ligand-protein complex geometry and the corresponding binding energy.

Results

The change in tryptophan fluorescence of spectrin indicates the association of the protein with imatinib, a non-fluorescent drug. Figure 1-4A shows characteristic fluorescence spectra of spectrin alone and in presence of varying concentration of imatinib. The inset of Figure 1-4A shows the progressive quenching of tryptophan fluorescence of spectrin upon the addition of increasing concentration of imatinib, thereby indicating the formation of a complex between spectrin and imatinib. Figure 1-4B shows the plot of the extent of fluorescence quenching as the function of imatinib concentration due to the association of imatinib and spectrin.

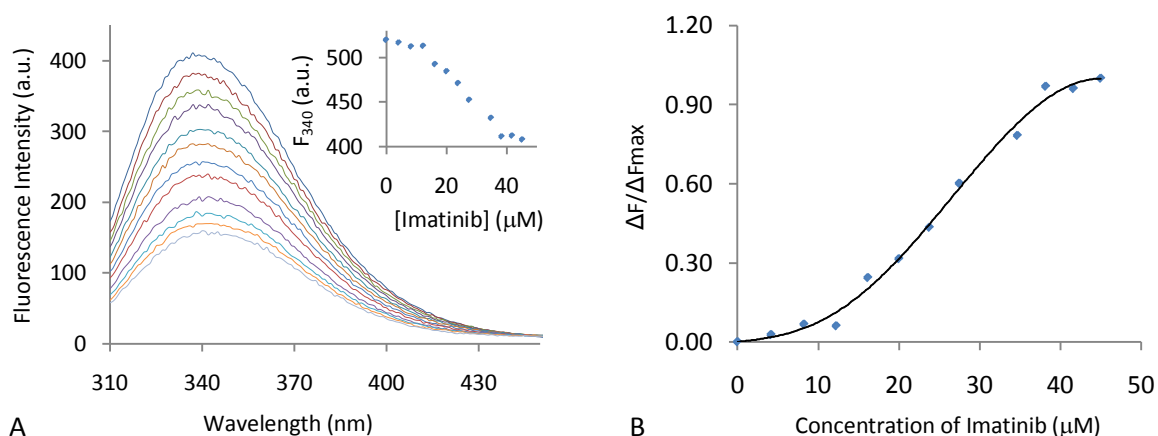


Figure 1-4: (A) Fluorescence emission spectra ($\lambda_{\text{ex}} = 295 \text{ nm}$) of $0.25 \mu\text{M}$ spectrin in 10 mM phosphate, 50 mM KCl buffer, $\text{pH } 7.4$, alone (blue line), and upon addition of increasing concentration of imatinib. Inset shows the binding isotherm (fluorescence intensity at 340 nm vs ligand concentration) for the interaction of spectrin with imatinib, after inner filter effect and volume correction. **(B)** Plot of the extent of imatinib-induced quenching vs concentration of imatinib.

The dissociation constant K_d was determined from double reciprocal plot at saturating conditions. The Figure 1-5A shows a representative double reciprocal plot of $1/\Delta F$ against $1/C_d$ to estimate K_d for imatinib binding to spectrin, which was found to be $5.8 \times 10^{-5} \text{ M}$ at 25°C .

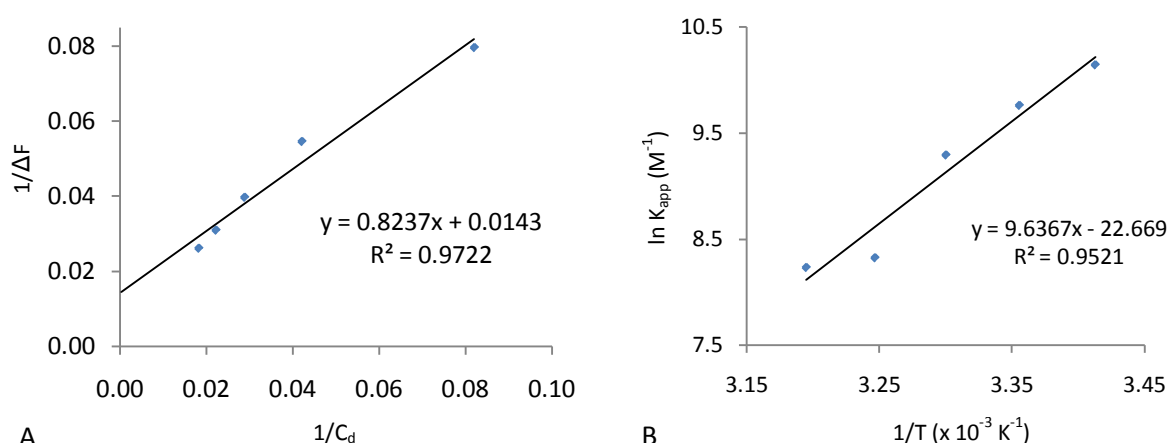


Figure 1-5: (A) The double reciprocal plot of $1/\Delta F$ against $1/C_d$ to evaluate K_d . **(B)** Van't Hoff plot for the interaction of spectrin ($0.05 \mu\text{M}$) with imatinib in 10 mM phosphate, 50 mM KCl buffer, $\text{pH } 7.4$.

Binding stoichiometry of about 120 was estimated from the extent of fluorescence quenching curve (Figure 1-4B). The thermodynamic parameters *e.g.* changes in free energy, enthalpy and entropy,

were evaluated from the variation of the apparent binding constant with temperature, the Van't Hoff plot. Figure 1-5B shows a representative Van't Hoff plot of $\ln K_{app}$ against $1/T$ for the interaction of imatinib with spectrin, *vide* Table 1-1. Thermodynamics parameters associated with the binding of imatinib and spectrin has been summarized in the Table 1-2.

Temperature	$K_{app} (M^{-1})$
293K	2.55×10^4
298K	1.74×10^4
303K	1.09×10^4
308K	4.13×10^3
313K	3.77×10^3

Table 1-1: Apparent binding constants with increasing temperature for the interaction of imatinib with erythroid spectrin (0.05 μ M) in 10mM phosphate, 50mM KCl buffer, pH 7.4.

Thermodynamic parameter	Value
ΔH	$-80.120 \text{ kJ M}^{-1}$
ΔS	$-188 \text{ J M}^{-1} \text{ K}^{-1}$
ΔG	$-24.096 \text{ kJ M}^{-1}$

Table 1-2: Thermodynamics parameters for the interaction of imatinib with erythroid spectrin (0.05 μ M) in 10 mM phosphate, 50 mM KCl buffer, pH 7.4.

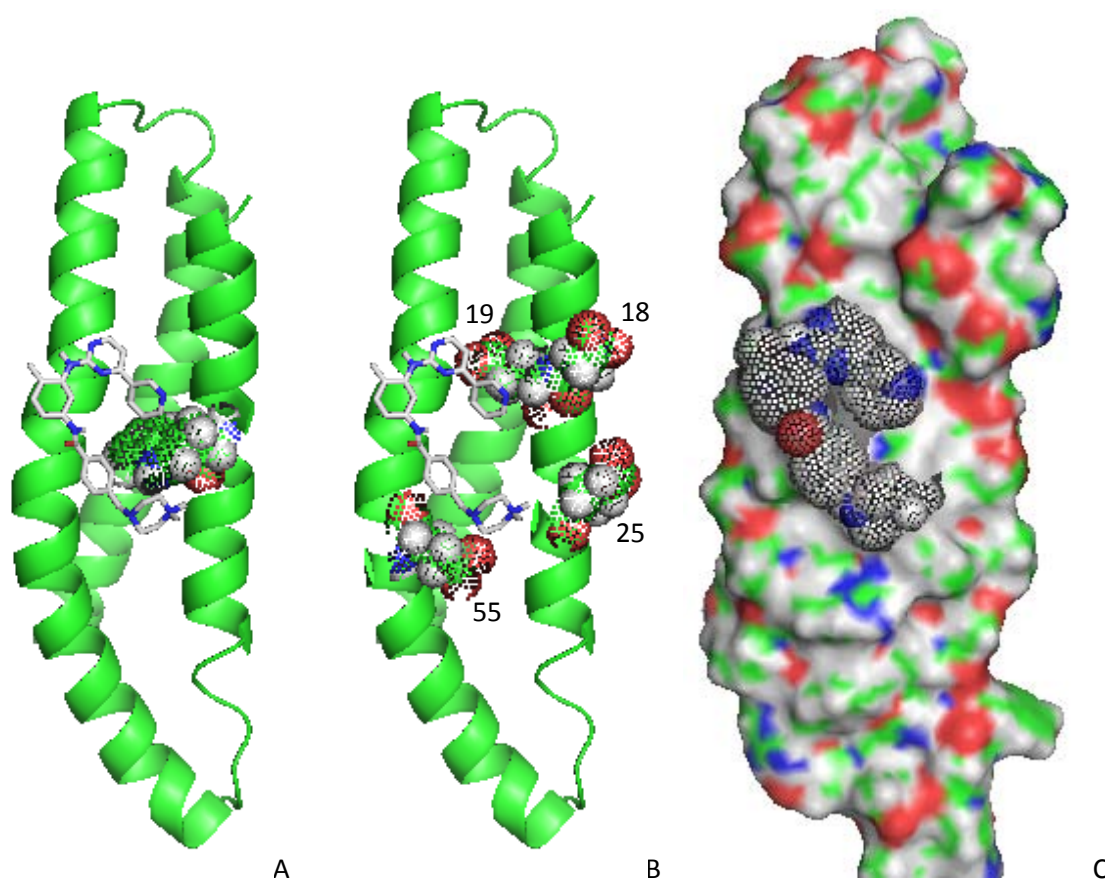


Figure 1-6: (A) shows the imatinib (shown in sticks) bound near the 22nd tryptophan residue of 16th repeat of α spectrin. (B) shows the amino acids with which imatinib is suggested to form hydrogen bonds; 18 is the aspartate , 19, 25, and 55 are glutamates. (C) shows the surface and dots model of the molecular dynamic simulation complex. Structure is generated in PyMOL Molecular Graphics System [26].

The geometry of imatinib (STI_ideal) complexed with the 16th repeat unit of chicken brain α spectrin (1AJ3), obtained in molecular docking study, has been shown in the Figure 1-6. The docking experiment suggested a binding near the 22nd tryptophan residue of this domain with an estimated

inhibition constant of 47.68 μM . The 95th tryptophan residue is inaccessible. Binding free energy was estimated to be $-24.686 \text{ kJ M}^{-1}$. Imatinib was suggested to interact with Asp 18, Glu 19, Glu 25, and Glu 55; *vide* Table 1-3 and Figure 1-7.

Interacting pair							
Ligand	N3 (12)	N1 (5)	N7 (32)	N6 (29)	N6 (29)	N1 (5)	N7 (32)
Protein	GLU19 (OE1)	ASP18 (OD1, OD2)	GLU25 (OE2)	GLU55 (OE2)	GLU25 (OE2)	GLU19 (OE2)	GLU55 (OE2)

Table 1-3: Interacting pair of atoms in the spectrin imatinib complex.

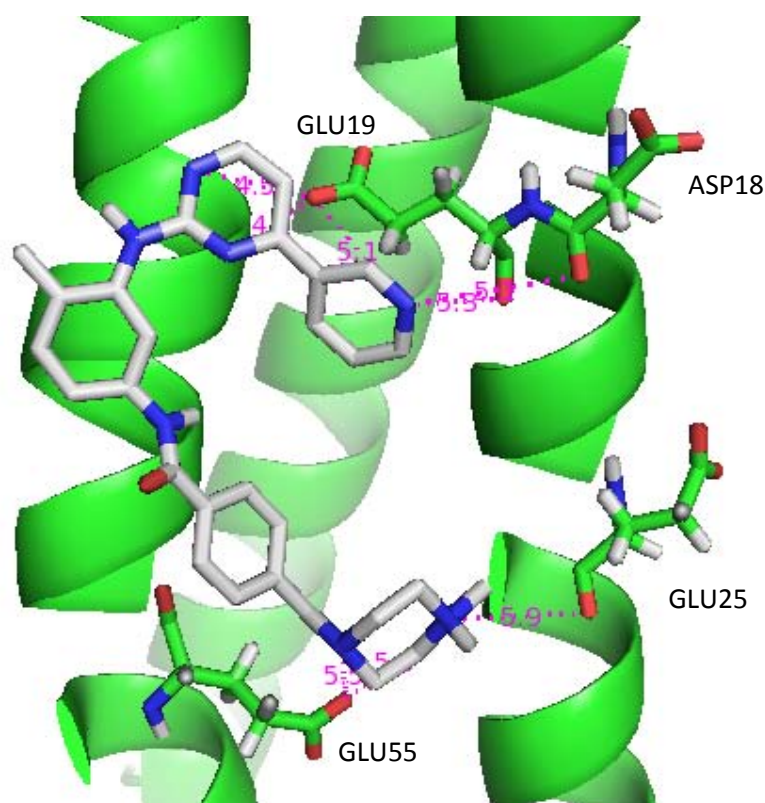


Figure 1-7: Interacting pair of atoms in the spectrin imatinib complex, with the distances labeled. Imatinib is shown in gray. All the distances lie between 4 to 6 Å. Structure is generated in PyMOL Molecular Graphics System [26].

Discussion

There are 42 tryptophan residues in each of the α and β subunits in the spectrin dimer, more than 90% of which are present in the 106 amino acid repeat units and their positions are conserved; 11th residue is partially and 45th residue is strongly conserved [27, 28]. The regular arrangement of tryptophan in the spectrin molecule makes them convenient intrinsic fluorescence reporter groups for monitoring conformational changes in spectrin that contribute to its elastic deformability exhibited in physiological conditions [29]. Many of the tryptophan residues are present at or in the vicinity of hydrophobic patches in spectrin, which can bind hydrophobic ligand and cause quenching of tryptophan fluorescence. Therefore, fluorescence quenching of tryptophan represents a convenient approach to monitor the binding of hydrophobic drugs to spectrin. Ovine erythroid spectrin, used in this study, has structural and self-associating properties that are indistinguishable from those of human and bovine spectrin [30]. Spectrin contains a unique binding site for hydrophobic fluorescence probes such as Prodan and pyrene [31, 32]. Spectrin also contains a large number of binding sites for fatty acid and its derivatives [33, 34], phospholipids [35], ATP [18] and the DNA binding antitumor antibiotics chromomycin and mithramycin [21] along the length of the large worm-like protein molecule.

The binding pattern (Figure 1-4A) suggests a positive cooperatively for the interaction between spectrin and imatinib. Binding dissociation constant, K_d was found to be $5.8 \times 10^{-5} M$ at 25°C, which is for Human Serum Albumin (HSA) corresponds to $\sim 3.3 \times 10^{-5} M$ [19]. Therefore, the binding affinity of imatinib to spectrin is comparable to that of HSA. Table 1-4 summarizes the binding data of other hydrophobic ligands to erythroid spectrin.

Hydrophobic Ligand	K_d (M)	Stoichiometry	Ref.
ATP	1.1×10^{-3}	50-100	[18]
2,3-DPG†	1.1×10^{-3}	50-100	
Dibucaine	3.5×10^{-5}	200	[22]
Ethidium bromide	1.3×10^{-5}	45-50	[21]
Chromomycin	5.0×10^{-6}	45-50	[21]
Mithramycin	2.6×10^{-6}	45-50	[21]
ANS	2.5×10^{-5}	4	[36]
Prodan	0.5×10^{-6}	1	[31, 36]
Pyrene	1.6×10^{-7}	1	[32]

Table 1-4: Binding of hydrophobic ligands to erythroid spectrin.
†Chakrabarti (unpublished observations).

Comparing the data in Table 1-4, with the imatinib binding data it appears that imatinib binds to spectrin with higher affinity than ATP. Binding stoichiometry (~ 120) is comparable to that of ATP, 2,3-DPG and Dibucaine. Imatinib fits in this table somewhere between ATP and Dibucaine.

Van't Hoff plot showed a positive slope or negative ΔH , indicating enthalpy driven process *i.e.* the heat content of the system, H is decreasing; exothermic

interaction. The binding occurs at the expense of free energy (ΔG) so process is thermodynamically favorable though the entropy is decreasing *i.e.* the system is getting more organized; *vide* Table 1-2.

As all the parameters showed negative sign (Table 1-2), hydrophobic interactions alone can not account for the stability of the association complexes. Reviewing the thermodynamic parameters characterizing self-association and ligand binding of proteins at 25°C it is not difficult to find ΔG , ΔH , and ΔS are all of negative sign; *vide* Table 1-5 [37]. Ross and Subramanian suggested a plausible mechanism of ligand binding under such circumstances [37]. According to this thermodynamic model, protein association occur in two steps; at first hydrophobic association causes the partial

The diagram illustrates the three stages of protein-ligand binding:

- A: Individually hydrated species**
 - Shows a large irregular shape labeled (PROTEIN) and a smaller irregular shape labeled (LIGAND).
- B: Hydrophobically associated**
 - Shows the protein and ligand in contact, with their outer boundaries overlapping.
 - Transitions from A to B are labeled:
 - PARTIAL IMMOBILIZATION: $\Delta G > 0$; $\Delta S < 0$; $\Delta C_p < 0$
 - HYDROPHOBIC: $\Delta G < 0$; $\Delta H > 0$; $\Delta S > 0$; $\Delta C_p < 0$
- C: Interacting complex**
 - Shows the protein and ligand fully integrated into a single complex.
 - Transitions from B to C are labeled:
 - ELECTROSTATIC INTERACTIONS: $\Delta G < 0$; $\Delta H \sim 0$; $\Delta S > 0$
 - VAN DER WAALS H-BONDS: $\Delta G < 0$; $\Delta H < 0$; $\Delta S < 0$; $\Delta C_p < 0$

As the ΔH value for spectrin imatinib binding is not near zero, it is not likely to be the electrostatic type of inter action rather Imatinib binding is likely to be stabilized by van der Waals type of interaction which also accounts for the decrease in binding affinity with the increasing temperature; *vide* Figure 1-8.

Ligand	ΔH (kJ M ⁻¹)	ΔS (J M ⁻¹ K ⁻¹)	ΔG (kJ M ⁻¹)
Lactic Dehydrogenase [38, 39]			
NAD ⁺	−26.359	−34.727	−15.899
NADH	−28.870	+7.113	−30.962
ADP-Ribose	−31.798	−41.840	−19.246
Idosalicyclic acid	−90.793	−255.224	−14.644
α -Chymotrypsin [40]			
proflavin	−46.024	−75.312	−25.104
indole	−62.760	−154.808	−17.991
N-Acetyl-D-Tryptophan	−79.496	−221.752	−13.807
Spectrin [22]			
Dibucaine	−11.900	−78.659	−6.300

Docking of imatinib (STI_ideal) to the 16th repeat unit of chicken brain α -spectrin (1AJ3) resulted with the inhibition constant of $4.8 \times 10^{-5} M$ and the binding free energy of $-24.686 kJ M^{-1}$, which goes very well with the experimentally obtained data of $5.8 \times 10^{-5} M$ and $-24.096 kJ M^{-1}$ respectively.

Conclusion

From all these studies, it can be concluded that spectrin imatinib interaction takes place. There is no unique binding site for Imatinib there like hydrophobic fluorescence probes such as ANS [36], Prodan [31, 36] and Pyrene [32]. Imatinib binds to the hydrophobic patches along the spectrin molecule. Partial immobilization due to hydrophobic association leading to the van der Waals or H-bonding type of interaction is likely to be the mechanism of binding.

Further experiments (absorption, Time Correlated Single Photon Counting, Laser Flash Photolysis) can be done to find out exact mechanism of quenching. Isothermal Titration Calorimetry (ITC) is required to establish the ligand receptor interaction. Circular Dichroism (CD) Spectroscopy provides information whether the ligand binding impart any conformational change to the protein molecule.

References

- [1] P.W. Manley, S.W. Cowan-Jacob, E. Buchdunger, D. Fabbro, G. Fendrich, P. Furet, T. Meyer, J. Zimmermann, **Imatinib: a selective tyrosine kinase inhibitor**, Eur. J. Cancer 38 (Suppl. 5) (2002) S19–S27.
- [2] E. Buchdunger, T. O'Reilly, J. Wood, **Pharmacology of imatinib (STI-571)**, Eur. J. Cancer 38 (Suppl. 5) (2002) S28–S36.
- [3] B. Nagar, W.G. Bornmann, P. Pellicena, T. Schindler, D.R. Veach, W.T. Miller, B. Clarkson, J. Kuriyan, **Crystal structures of the kinase domain of c-Abl in complex with the small molecule inhibitors PD173955 and imatinib (STI-571)**, Cancer Res. 62 (2002) 4236–4243.
- [4] U. Rix, O. Hantschel, G. Durnberger, L.L. Remsing Rix, M. Planyavsky, N.V. Fernbach, I. Kaupe, K.L. Bennett, P. Valent, J. Colinge, **Chemical proteomic profiles of the BCR-ABL inhibitors imatinib, nilotinib, and dasatinib reveal novel kinase and nonkinase targets**, Blood 2007, 110(12):4055-4063.
- [5] M. Bantscheff, D. Eberhard, Y. Abraham, S. Bastuck, M. Boesche, S. Hobson, T. Mathieson, J. Perrin, M. Raida, C. Rau, **Quantitative chemical proteomics reveals mechanisms of action of clinical ABL kinase inhibitors**, Nat Biotechnol 2007, 25(9):1035-1044.
- [6] C.L. Sawyers, **Chronic myeloid leukemia**, N Engl J Med 1999, 340(17):1330-1340.
- [7] T.G. Lugo, A.M. Pendergast, A.J. Muller, O.N. Witte, **Tyrosine kinase activity and transformation potency of bcr-abl oncogene products**, Science 1990, 247(4946):1079-1082.
- [8] C.L. Sawyers, **Molecular consequences of the BCR-ABL translocation in chronic myelogenous leukemia**, Leukemia Lymphoma 1993, 11(Suppl 2):101-103.
- [9] Deininger M, Buchdunger E, Druker BJ, **The development of imatinib as a therapeutic agent for chronic myeloid leukemia**, Blood 2005, 105(7):2640-2653.
- [10] O. Hantschel, U. Rix, G. Superti-Furga, **Target spectrum of the BCR-ABL inhibitors imatinib, nilotinib and dasatinib**, Leukemia Lymphoma 2008, 49(4):615-619.
- [11] B. Nagar, O. Hantschel, M.A. Young, K. Scheffzek, D. Veach, W. Bornmann, B. Clarkson, G. Superti-Furga, J. Kuriyan, **Structural basis for the autoinhibition of c-Abl tyrosine kinase**, Cell 2003, 112(6):859-871.
- [12] T. Schindler, W. Bornmann, P. Pellicena, W.T. Miller, B. Clarkson, J. Kuriyan, **Structural mechanism for STI-571 inhibition of Abelson tyrosine kinase**, Science 2000, 289(5486):1938-1942.
- [13] B. Alberts, A. Johnson, J. Lewis, M. Raff, K. Roberts, P. Walter, **Molecular Biology of the Cell**, 4ed:601-603.
- [14] D. W. Speicher, V.T. Marchesi, **Erythrocyte spectrin is comprised of many homologous triple helical segments**, Nature 1984, 311:177-180.

- [15] D.M. Shotton, B.E. Burke, D. Branton, **The molecular structure of human erythrocyte spectrin: biophysical and electron microscopic studies**, J. Mol. Biol. 1979, 131:303-329.
- [16] T.J. Byers, D. Branton, **Visualization of the protein associations in the erythrocyte membrane skeleton**, Proc. Natl. Acad. Sci. USA 1985 82:6153-6157.
- [17] Novartis, **Gleevec® Prescription Information**, www.gleevec.com/prescription-information.jsp.
- [18] A. Chakrabarti, S. Bhattacharya, S. Ray, M. Bhattacharyya, **Binding of a Denatured Heme Protein and ATP to Erythroid Spectrin**, Biochemical and Biophysical Research Communications 2001, 282(5):1189-1193.
- [19] I. Fitos, J. Visy, F. Zsila, G. Mády, M. Simonyi, **Selective binding of imatinib to the genetic variants of human α_1 -acid glycoprotein**, Biochimica et Biophysica Acta 2006, 1760:1704–1712.
- [20] W.B. Gratzer, **Methods Enzymol**, 1982, 85:475-480.
- [21] S. Majee, D. Dasgupta, A. Chakrabarti, **Interaction of the DNA-binding antitumor antibiotics, chromomycin and mithramycin with erythroid spectrin**, Eur. J. Biochem. 1999, 260:619-626.
- [22] M. Mondal, A. Chakrabarti, **The tertiary amine local anesthetic dibucaine binds to the membrane skeletal protein spectrin**, FEBS Letters 2002, 532:396-400.
- [23] J.R. Lakowicz, **Principles of Fluorescence Spectroscopy**, 2ed:53-54.
- [24] M. Bhattacharya, C. Mukhopadhyay, A. Chakrabarti, **Specificity of Prodan for the Self-associating Domain of Spectrin: A Molecular Docking Study**, Journal of Biomolecular Structure & Dynamics 2006, 24(3):269-276.
- [25] Z. Bikadi, S. Kovacs, L. Demko, E. Hazai, **DockingServer (www.dockingserver.com)**, Virtua Drug Ltd. Budapest, Hungary (2007).
- [26] L.W. DeLano, **The PyMOL Molecular Graphics System**, DeLano Scientific LLC, USA 2008, v1.1r1:<http://www.pymol.org>.
- [27] K.E. Sahr, P. Laurila, L. Kotula, A.L. Scarpa, E. Coupal, T.L. Leto, A.J. Linnenbach, J.C. Winkelmann, D.W. Speicher, V.T. Marchesi, P.J. Curtis, B.G. Forget, **The complete cDNA and polypeptide sequence of human erythroid α -spectrin**, J. Biol. Chem. 1990, 265:4434-4443.
- [28] J.C. Winkelmann, J.G. Chang, W.T. Tse, A.L. Scarpa, V.T. Marchesi, B.G. Forget, **Full length sequence of the cDNA for human erythroid β -spectrin**, J. Biol. Chem. 1990, 265:11827-11832.
- [29] N.K. Subbarao, R.C. MacDonald, **Fluorescence studies of spectrin and its subunits**, Cytoskel. 1994, 29:72-81.
- [30] N. Cole, G.B. Ralston, **The self-association of ovine erythrocyte spectrin**, Int. J. Biochem. 1993, 25(11):1555-1559.

- [31] A. Chakrabarti, **Fluorescence of spectrin-bound Prodan**, Biochemical and Biophysical Research Communications 1996, 226:495-497.
- [32] M.E. Haque, S. Ray, A. Chakrabarti, **Polarity estimate of the hydrophobic binding sites in erythroid spectrin: a study of pyrene fluorescence**, J. Fluoresc 2000, 10:1-6.
- [33] H. Isenberg, J.G. Kenna, N.M. Green, W.B. Gratzer, **Binding of hydrophobic ligands to spectrin**, FEBS Letters 1981, 129:109-112.
- [34] E. Kahana, J.C. Pinder, K.S. Smith, W.B. Gratzer, **Fluorescence quenching of spectrin and other red cell membrane cytoskeletal proteins: Relation to hydrophobic binding sites**, Biochem J. 1992, 282:75-80.
- [35] W. Diakowski, A. Prychidny, M. Swistak, M. Nietubye, K. Bialkowska, J. Szopa, A.F. Sikorski, **Brain spectrin (fodrin) interacts with phospholipids as revealed by intrinsic fluorescence quenching and monolayer experiments**, Biochem J. 1999, 338:83-90.
- [36] M. Bhattacharyya, S. Ray, S. Bhattacharya, A. Chakrabarti, **Chaperone Activity and Prodan Binding at the Self-associating Domain of Erythroid Spectrin**, J. Biol. Chem. 2004, 279:55080-55088.
- [37] P.D. Ross, S. Subramanian, **Thermodynamics of Protein Association Reactions: Forces Contributing the Stability**, Biochemistry 1981, 20:3096-3102.
- [38] S. Subramanian, P.D. Ross, **Calorimetric investigation of NAD binding to some dehydrogenases**, Biochem Biophys Res Commun. 1977, 78(1):461-466.
- [39] S. Subramanian, P.D. Ross, **Thermodynamics of binding of oxidized and reduced nicotinamide adenine dinucleotides, adenosine-5'-diphosphoribose, and 5'-iodosalicylate to dehydrogenases**, Biochemistry 1978, 17(11):2193-2197
- [40] D.D. Shiao, J.M. Sturtevant, **Calorimetric investigations of the binding of inhibitors to alpha-chymotrypsin. I. The enthalpy of dilution of alpha-chymotrypsin and of proflavin, and the enthalpy of binding of indole, N-acetyl-D-tryptophan, and proflavin to alpha-chymotrypsin**, Biochemistry 1969 8(12):4910-4917.

off the track

Understanding UV-Visible Spectroscopy

with Professor Samita Basu

Chemical Science Division

Saha Institute of Nuclear Physics, Kolkata

When light passes through the media a portion of the light may be absorbed. Coloured solution absorbs visible light and that is why it appears coloured. Colourless benzene absorbs in the near ultraviolet. Had human eye been sensitive to this region of spectrum, benzene would have appeared intensely coloured.

What happens to this absorbed light?

Normally an atom or a molecule is in the lowest energy level (Ground electronic state). When it absorbs a quantum of light, an electron is promoted from an occupied orbital to an unoccupied orbital of greater potential energy (Excited electronic state of the molecule). Generally the most probable transition is from the highest occupied molecular orbital (HOMO) to lowest unoccupied molecular orbital (LUMO).

Ultraviolet and visible light (200–800nm) causes electronic excitation. Infrared causes vibrational excitation and long infrared and microwave, the rotational excitation. So, it implies, simple rotation and vibrational excitation needs very small amount of energy and thus, the corresponding spectral line is far out in the longer wavelength region. On the other hand, electronic transition needs more energy. It is often accompanied with vibrational and rotational excitation.

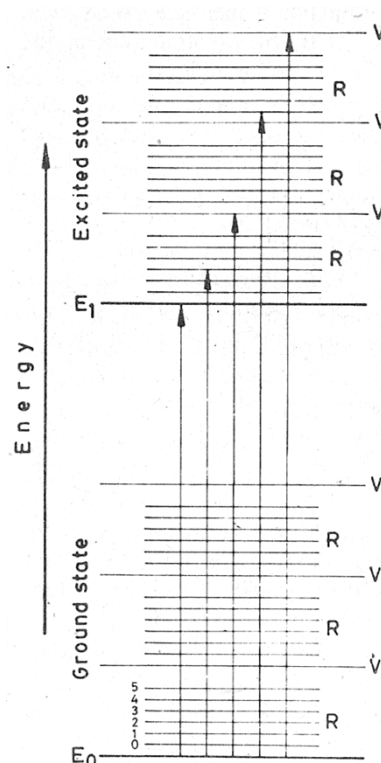


Figure 2-1: Energy-level diagram. V, vibrational and R, rotational levels.

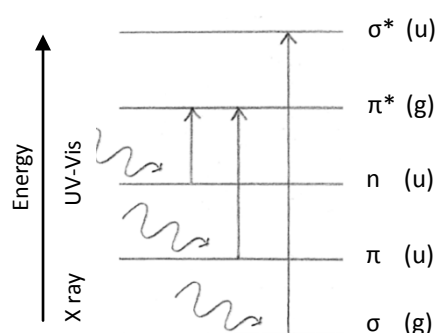


Figure 2-2: Plausible electronic transitions. g, gerade and u, ungerade wave functions

UV-Visibel light causes the $\pi \rightarrow \pi^*$ and $n \rightarrow \pi^*$ transitions. Due to high energy gap X ray is required for the $\sigma \rightarrow \sigma^*$ transition.

As stated earlier, the simple electronic transitions are associated with the vibrational and rotational excitations. There are some selection rules (Franck-Condon Principle) in operation:

1. Electronic selection rule
2. vibrational selection rule
3. spin selection rule

The first two are coupled, called the vibronic selection rule. This principle is based on the assumption that transition from one energy state to another is so rapid (in femtosecond order) that the nuclei of the atoms involved can be considered to be stationary during the transition (Born-Oppenheimer approximation). The probability amplitude for the electronic transition between two states is given by transition moment integral,

$$\langle \psi' | e\vec{r} + \vec{\mu} | \psi \rangle = \langle \psi' | e\vec{r} | \psi \rangle + \langle \psi' | m\vec{v}\vec{r} | \psi \rangle \quad (\text{Orbital selection rule})$$

If we operate an inversion operator, for centrosymmetric molecules (viz. benzene), the first term in this expression due to electric dipole will not allow $g \rightarrow g$ and similarly $u \rightarrow u$ transitions but the

second term that is due to magnetic dipole do. Usually, $g \leftrightarrow u$ transitions take place. (g, gerade or symmetric wave function and u, ungerade or asymmetric wave function)

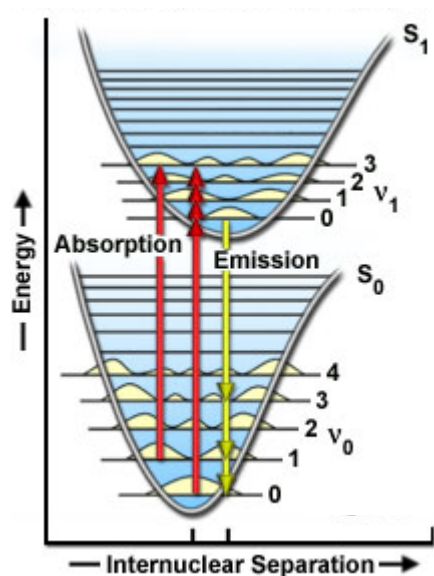


Figure2-3: Franck-Condon Energy Diagram.

Under ideal situations $0 \rightarrow 0$ vibronic transition is the most probable one followed by $0 \rightarrow 1$, $0 \rightarrow 2$... but due to the vibration and collisions the τ_e is displaced favoring some other transition over $0 \rightarrow 0$ transition. According to the Figure 2-3 in both the excitation and relaxation processes $0 \rightarrow 1$ transition is more probable than $0 \rightarrow 0$ transition and so does reveal in the spectral pattern (*vide* Figure 2-4A and 2-9A, the absorption and emission spectra of anthracene showing five distinct vibronic transitions)

Two major applications of light absorption are UV-Visible spectroscopy and IR spectroscopy. Here our concern lies with the first one.

During an electronic transition, a change from one vibrational level to another will be more likely to happen if the two vibrational wave functions overlap more significantly. It is given by the overlap integral, $\langle \psi_f^{v'} | \psi_i^v \rangle = \delta$. It gives the binary probability; $\delta = 0$ when $v \neq v'$ and $\delta = 1$ when $v = v'$.

Similarly, the spin selection rule is given by $\langle \psi_f^s | \psi_i^s \rangle = \delta$, indicating *singlet* \rightarrow *singlet* transition is allowed but *singlet* \leftrightarrow *triplet* transitions are not (phenomenon of phosphorescence will be discussed in due course).

Absorption Spectroscopy

Absorption spectroscopy is widely used for analytical purposes; it is based on the Beer-Lambert law: if a beam of light of intensity I_0 passes through a solution of concentration c contained in a transparent cell of thickness d , the emergent beam will be weaker in intensity than the incident beam due to absorption. If the intensity of emergent beam is I , it is given by the following relation.

$$\ln(I/I_0) = \lambda cd$$

To avoid complications due to exponential nature of the relation, Beer's law is generally used in the logarithmic form after conversion to base 10 when it becomes

$$\log(I_0/I) = (\lambda/2.303) c \cdot d$$

On writing O.D. (optical density or absorbance) for $\log(I_0/I)$ and ϵ for $\lambda/2.303$, ϵ being a constant called molar extinction coefficient or molar absorptivity provided c is expressed in molarity, the following shortest form of Beer-Lambert law is obtained:

$$[O.D.] = \epsilon \cdot c \cdot d$$

The slope of the plot O.D. against concentration gives the value of ϵ when the path length is unity. Therefore, ϵ is a physical property of the sample, the hallmark for its purity.

Some features of Optical Density

- As I_0 is always greater than I , O.D. is always greater than zero.
- $O.D. = 1$ means that the emergent light is one tenth as intense as incident light.
- Optical Density is an additive property. i.e. Optical Density of a mixture having A, B, and C will be equal to the sum of the Optical Densities due to A, B, and C individually provided A, B, and C are noninteractive.

Study of absorption spectroscopy with anthracene as a standard sample

Anthracene in acetonitrile solvent showed five distinct peaks in the absorption spectra. These are the representatives of five different $\pi \rightarrow \pi^*$ vibronic transitions. Absorptions at 357 nm were plotted against the concentration to obtain the extinction coefficient of anthracene. It was found to be $11800 \text{ mole}^{-1} \text{ lit. cm}^{-1}$.

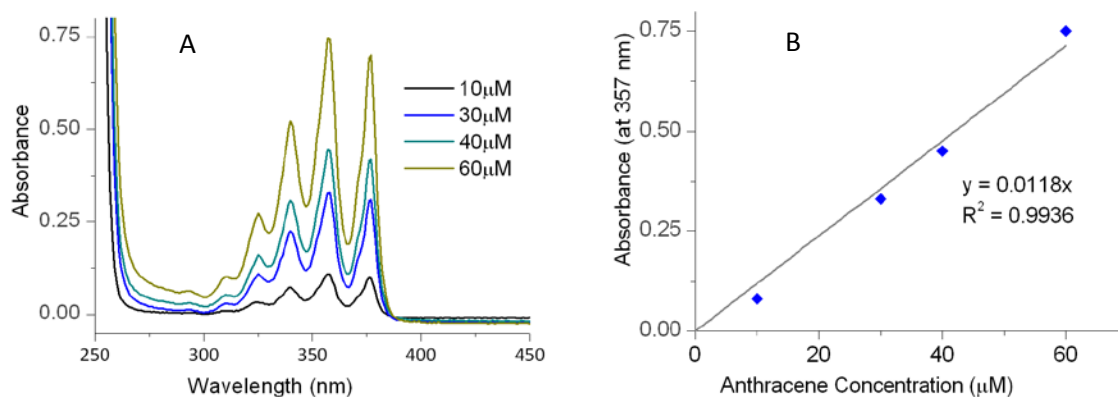
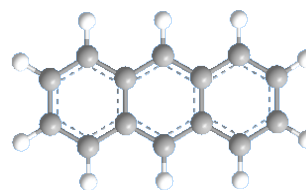


Figure 2-4: (A) represents the absorption spectra of anthracene with increasing concentration and (B) is the absorbance versus concentration plot. The structure of anthracene was drawn in Chem3D Pro v11.0 (ChembridgeSoft).

Absorption of a protein, spectrin

Electronic molar absorption spectrum of spectrin, an erythroid cytoskeletal protein, showed two absorption maxima within the range of 250 nm to 350 nm (Figure 2-5); the major peak appeared near 280 nm due to both the tryptophan and tyrosine residues present in the proteins and another peak (which is revealed in the second derivative curve) near 295 nm exclusively due to tryptophan residues. The absorption maxima for tryptophan are 280 and 295 nm and it is for tyrosine is 274 nm.

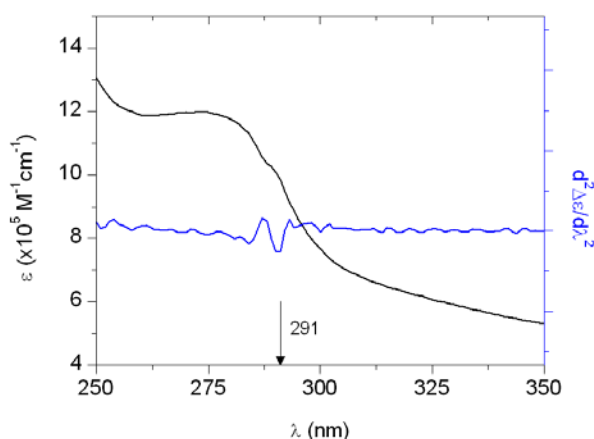
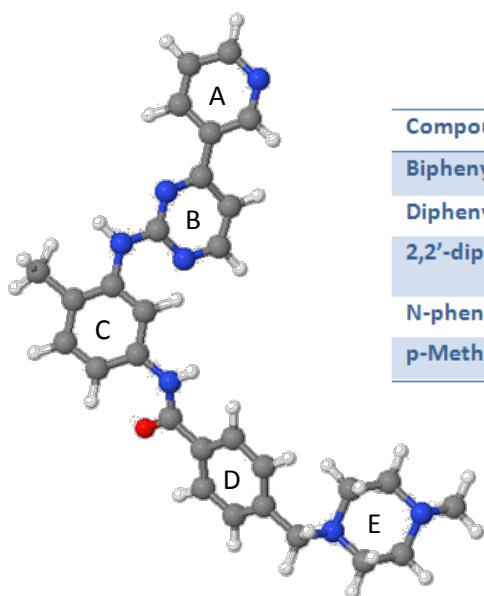


Figure 2-5: Absorption spectrum of spectrin, an erythroid cytoskeletal protein.

Analysis of electronic absorption spectra of imatinib

From spectroscopic point of view, imatinib (4-(4-methyl-piperazin-1-yl-methyl)-N-[4-methyl-3-(4-pyridin-3-yl-pyrimidin-2-yl-amino)-phenyl]-benzamide methanesulfonate), an anti-leukemia drug, possesses a *composite chromophoric system* which displays several electronic transitions. Using a simplified, qualitative description, the UV spectrum of imatinib can be approximated by the superposition of the spectra of a biphenyl (A+B), a diphenylamine (B+C) and an N-phenyl-benzamide (C+D) units being in partial π - π^* conjugation with each other [1]. Based on literature data, properties of the main $\pi \rightarrow \pi^*$ electronic transitions of these chromophoric units are summarized in the following table (Figure 2-6).



Compound	λ_{\max} (nm)	ϵ_{\max} ($M^{-1} \text{ cm}^{-1}$)	Solvent	Ref.
Biphenyl	248	16600	Water	[2]
Diphenylamine	282.2	20400	Acetonitrile	[3]
2,2'-dipyridylamine	265 312	25000 19000	EtOH	[4]
N-phenyl-benzamide	262	14500	Acetonitrile	[5]
p-Methyl-benzamide	238	11500	Water	[6]

Figure 2-6: This structure of imatinib was retrieved from PDB (ID: STI_ideal) and the model was generated with Jmol v11.7.46. The table shows absorption data of different chromophoric units

Consequently, intensity and energy of these bands vary by different degrees upon conjugation of the chromophoric parts in the imatinib molecule resulting in a complex, mixed band system. In the UV spectrum of imatinib recorded in acetonitrile, only two maxima can be distinguished but both

consist of several overlapping sub-bands as demonstrated by series of minima in the second derivative curve.

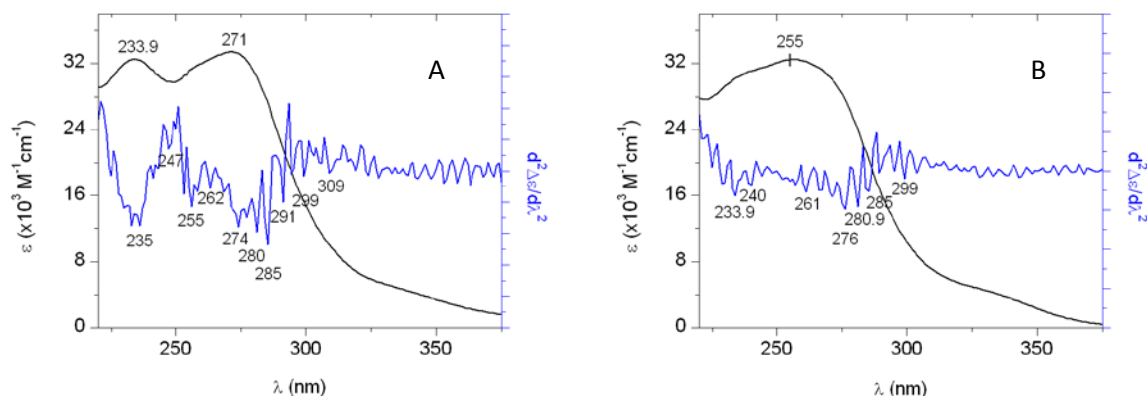


Figure 2-7: Electronic molar absorption spectra of imatinib mesilate in different media, (A) is the spectrum taken in acetonitrile, at 25°C and (B) was taken in phosphate buffer pH 7.4, at 25°C. Double derivative curves of imatinib spectra are also shown.

It is likely that the 234 nm peak corresponds dominantly to the pyridylpyrimidine fraction (A+B) and it also has some contribution from the p-methyl benzamide moiety (D ring). The band centered at 271 nm belongs to the pyrimidyl–phenylamine unit (B+C) and contains contributions from the N-phenyl benzamide moiety (C+D), too. The weak absorption around 310 nm may also be assigned to the heteroaromatic–aromatic substituted amine moiety (B+C)[4]. In phosphate buffer imatinib has one broad peak with maximum at 255 nm. The second derivative curves revealed that it cannot be considered as a largely blue shifted peak centered at 271 nm in organic solvents. In fact the electronic transitions at 275–285nm range belonging to the (B+C) unit show only slight shift, in accordance with the literature data revealing slight solvent effect for analogous molecules [3, 4, 7]. It can be assumed that the absorbance due to the (C+D) part at 255 nm is more intense in aqueous solvent.

Relaxation mechanism for the excited state molecules

Electron from the excited electronic state eventually returns to the ground electronic state and the energy may be released as a photon (radiative relaxation) or be dissipated by other non-radiative ways or as a combination of the two. The same selection rules as the excitation are applicable here in the relaxation mechanism. All these electronic transitions are summarized in a simplified diagram, called the Jablonski energy diagram (after its first depictror), shown below.

Vibrational relaxation, the most common of the non-radiative decay processes, occurs very rapidly ($< 10^{-12}$ seconds) and is enhanced by physical contact of an excited molecule with other particle and energy, in the form of vibrations and rotations, can be transferred through collisions. This means the most excited state molecules never emit any energy because in liquid samples the solvent or, in gas phase samples, other gas phase molecules that are present *steal* the energy before other deactivation processes can occur. *Internal conversion* is the radiationless transition between excited energy states of the same spin. The diagram also suggests the *inter system crossing*, i.e the transition between singlet and triplet states, which according to the spin selection rule was overruled earlier.

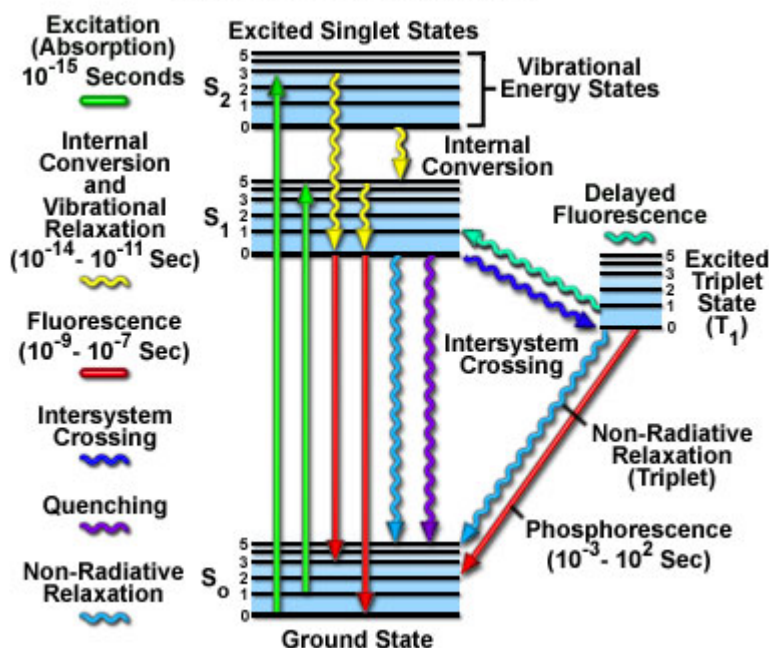
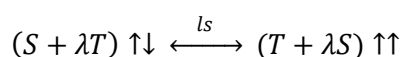


Figure 2-8: Jablonski energy diagram.

Internal conversion is the radiationless transition between excited energy states of the same spin. The diagram also suggests the *inter system crossing*, i.e the transition between singlet and triplet states, which according to the spin selection rule was overruled earlier.

So, what accounts for this inter system crossing?

Due to the spin orbit coupling, singlet state gets a partial triplet characteristic and vice-versa. When the extent of this spin orbit coupling (λ) is very high, as in the presence of heavy atoms, *singlet* \leftrightarrow *triplet* transitions may take place.



Photon emission due to $S_n \rightarrow S_0$ transitions is termed *fluorescence* and it is for $T_n \rightarrow S_0$ transitions is called *phosphorescence*. The lifetimes of fluorescence states are very short ($10^{-9} - 10^{-7}$ seconds) making it statistically more likely than the phosphorescence, lifetime of which is somewhat longer (10^{-3} seconds to several minutes).

Quantum yield

The fluorescence quantum yield is defined as the ratio of the number of photons emitted to the number of photons absorbed. Substances with the largest quantum yields, approaching unity, such

as rhodamines, display the brightest emission. Experimentally, relative fluorescence quantum yields can be determined by measuring fluorescence of a fluorophore of known quantum yield with the same experimental parameters (excitation wavelength, slit widths, photomultiplier voltage etc.) as the substance in question. The quantum yield is then calculated by:

$$\Phi_s = \Phi_r \times \left(\frac{\text{Grad}_s}{\text{Grad}_r} \right) \left(\frac{\eta_s^2}{\eta_r^2} \right)$$

Where the subscripts r and s denote reference and sample respectively, Φ is the fluorescence quantum yield, *Grad* the gradient from the plot of integrated fluorescence intensity over the emission range vs absorbance, and η the refractive index of the solvent. *vide* references for the determination of absolute quantum yields.

Fluorescence spectroscopy

Fluorescence spectroscopy analyses the *emission spectra* of a fluorescent species called the fluorophore. In a typical experiment, the different frequencies of fluorescent light emitted by a sample are measured, holding the excitation light at a constant wavelength (the spectrum obtained is called the emission spectrum). Fluorescence intensities are measured in arbitrary unit and it is machine dependent.

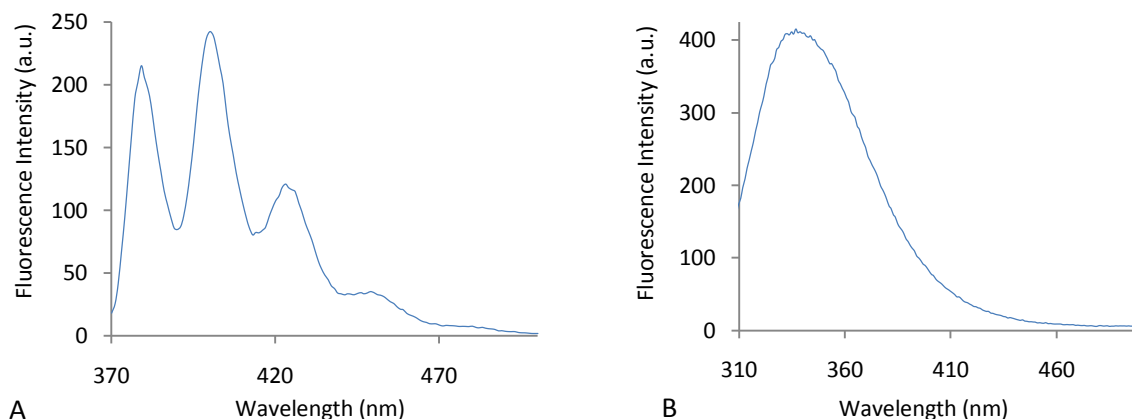


Figure 2-9: (A) emission spectrum of anthracene in acetonitrile solvent, ($\lambda_{\text{ex}} = 357 \text{ nm}$); (B) emission spectrum of spectrin tryptophan ($\lambda_{\text{ex}} = 295 \text{ nm}$) in phosphate buffer, pH 7.4. excitation and emission slits were kept at 5 nm and 10 nm respectively.

Excited molecule loses vibrational energy until it reaches the lowest vibrational state of the excited electronic state. The molecule then drops down to one of the various vibrational levels of the ground electronic state (Figure 2-10), emitting a photon in the process. As molecules may drop down into any of the vibrational levels of the ground state, the photons will have different energies, and thus frequencies; it is suggestive of the structure of different vibrational levels.

Fluorescence measurements can be broadly classified into two types of measurements, steady-state and time-resolved. Steady-state measurements are those performed with constant illumination and observation. This is the most common type of measurement. The sample is illuminated with a continuous beam of light, and the intensity or emission spectrum is recorded. Because of the nanosecond timescale of fluorescence, most measurements are steady-state measurements. When the sample is first exposed to light, steady state is reached almost immediately. The second type of measurements, time-resolved measurements, is used for measuring *intensity decays* or *anisotropy decays* (vide Appendix). For these measurements, the sample is exposed to a pulse of light, where the pulse width is typically shorter than the decay time of the sample. This intensity decay is recorded with a high-speed detection system that permits the intensity or anisotropy to be measured on the nanosecond timescale.

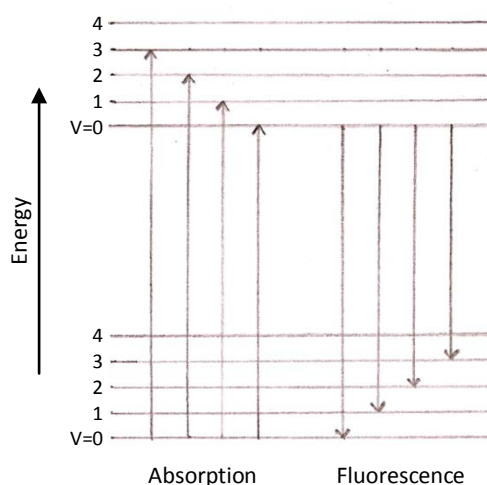


Figure 2-10: Vibronic transitions during excitation and emission.

There exists a simple relationship between steady-state and time-resolved measurements. The steady-state observation is simply an average of the time-resolved phenomena over the intensity decay of the sample. But, it turns out that much of the molecular information available from fluorescence is lost during the time-averaging process, accounting for the requirement of more complex and expensive time resolved experiments.

Excitation spectrum

Emission spectra is typically independent of excitation wavelength (Kasha's rule). If a particular emission wavelength, preferably the emission maximum or one of the maxima, is monitored for a range of excitation wavelength, it generates a pattern depicting the relative emission of the fluorophore at each excitation wavelength. It is called the excitation spectrum. Normalized excitation spectra of a fluorophore are super imposable on its normalized absorption spectra, provided excited state geometry remains the same.

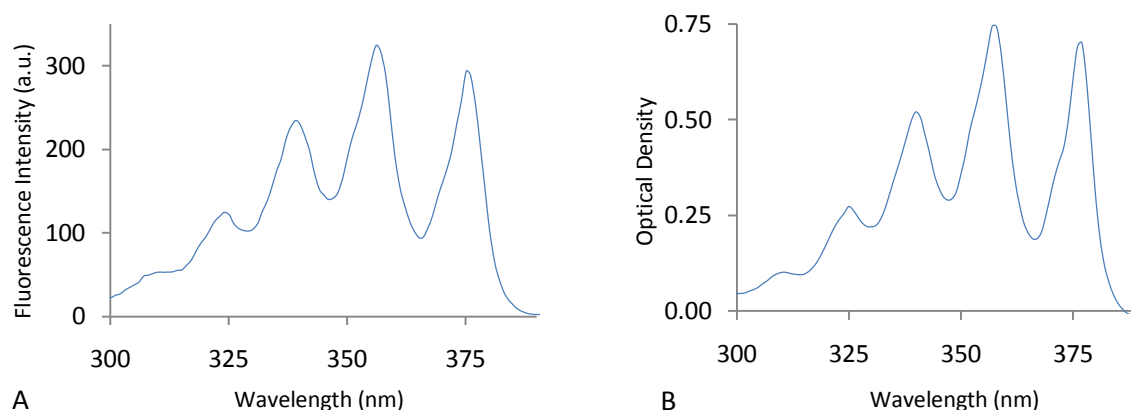


Figure 2-11: (A) Excitation spectrum ($\lambda_{em} = 400$ nm) of anthracene in acetonitrile solvent. (B) Absorption spectrum of anthracene ($60 \mu\text{M}$) in acetonitrile solvent.

A fluorescence excitation spectrum is more sensitive method of obtaining the absorption pattern and has great analytical value in systems containing a number of fluorescent species or large background absorption.

Stokes' shift

Jablonski diagram suggests that except the $0 \rightarrow 0$ transitions the energy of the emission is typically less than that of absorption. Hence, fluorescence typically occurs at lower energies or longer wavelengths. This phenomenon is called Stokes' shift (after Sir G. G. Stokes)

One common cause of the Stokes' shift is the rapid decay to the lowest vibrational level of S_1 . In addition to this, fluorophores can display further Stokes' shifts due to solvent effects (*solvent relaxation*; vide Appendix), excited-state reactions, complex

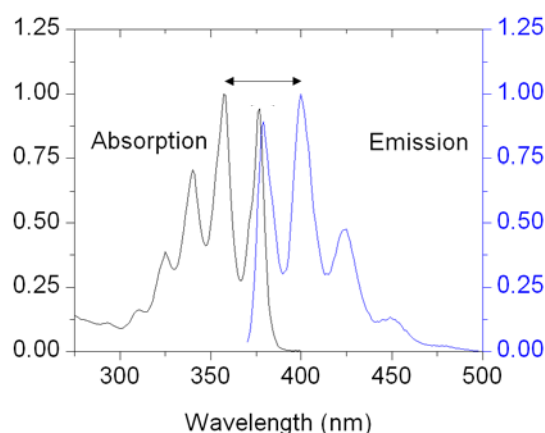


Figure 2-12: Normalized absorption and emission spectra of anthracene in acetonitrile solvent demonstrating the Stokes' shift (shown by arrow).

formation, and/or energy transfer.

Mirror image relationship

It has been stated earlier that electronic transitions due to absorption are often accompanied with vibrational excitation and during the relaxation process also electron from the lowest vibrational level of the first excited state may jump to any of the vibrational levels of the ground state emitting a photon. Besides, the same selection rules are in operation in both the cases. Therefore, it suggests, theoretically, the absorption and emission spectra to be the mirror image of each other.

Although the mirror image rule often holds, many exceptions to this rule occur. Such deviations from the mirror image rule usually indicate a different geometric arrangement of nuclei in the excited state as compared to the ground state. Nuclear displacements can occur prior to emission because of the relatively long lifetime of the S_1 state, which allows time for motion following the instantaneous process of absorption.

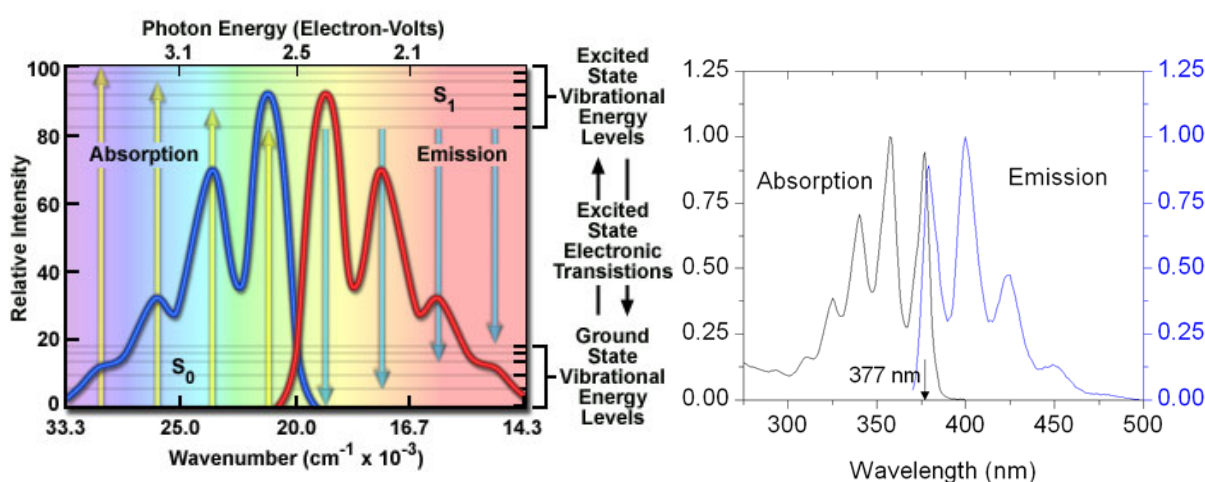


Figure 2-13: (A) Schematic representation of the mirror image rule. (B) normalized absorption and excitation spectra of anthracene ($10 \mu\text{M}$) in acetonitrile solvent. Excitation spectrum was recorded at emission 400 nm keeping the excitation and emission slits at 10 and 5 nm respectively. Emission spectrum was recorded at excitation 357 nm and keeping the emission and excitation slits at 10 and 5 nm respectively.

0 – 0 band energy

From the Figure 2-13B 0 – 0 band energy can easily be calculated. The peaks representing the $0 \rightarrow 0$ transitions, ideally should overlap exactly. Here, the transitions corresponds to 377 nm wavelength. Using $E = hc/\lambda$, the 0 – 0 band energy for anthracene appears to be $5.27 \times 10^{-19} \text{ Joule}$ or 3.3 eV.

Fluorescence quenching

Decrease in fluorescence intensity or the fluorescence quenching can occur by different mechanisms. *Collisional quenching*, also known as the *dynamic quenching*, occurs when the excited-state fluorophore is deactivated upon contact with some other molecule in solution, which is called the quencher. Collisional quenching is illustrated on the modified Jablonski diagram in Figure 2-14. In this case the fluorophore is returned to the

ground state during a diffusive encounter with the quencher without emitting any photon. The molecules are not chemically altered in the process. For collisional quenching, the decrease in intensity is described by the well-known *Stern-Volmer equation*:

$$\frac{F_0}{F} = 1 + K[Q]$$

In this expression K is the Stern-Volmer quenching constant, and $[Q]$ is the quencher concentration. F_0/F is expected to be linearly dependent upon the concentration of quencher. A plot of F_0/F versus $[Q]$ yields an intercept of 1 on the y-axis and a slope equal to K . A linear Stern-Volmer plot is generally indicative of a single class of fluorophore, all equally accessible to quencher. If two fluorophore populations are present, and one class is not accessible to quencher, then the Stern-Volmer plots deviate from linearity towards the x-axis. This result is frequently found for the quenching of tryptophan fluorescence in proteins by polar or charged quenchers. These molecules do not readily penetrate the hydrophobic interior of proteins, and only those tryptophan residues on the surface of the protein are quenched. It is important to recognize that observation of a linear Stern-Volmer plot does not prove that collisional quenching of fluorescence has occurred.

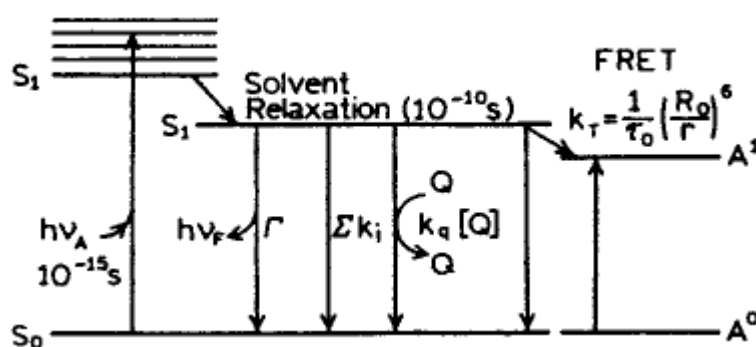


Figure 2-14: Modified Jablonski diagram showing few mechanisms of fluorescence quenching, non-radiative decay (Σk_i), collisional quenching (Q , quencher), and fluorescence resonance energy transfer (A , acceptor). For solvent relaxation, vide appendix.

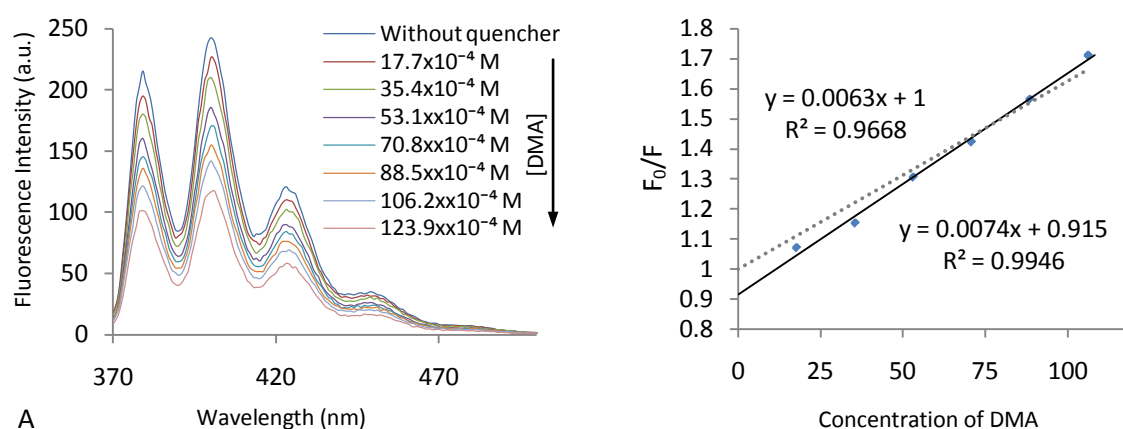


Figure 2-15: (A) fluorescence quenching of anthracene (10 μM) with increasing concentrations of dimethylaniline (DMA). (B) Stern-Volmer plot for the fluorescence quenching of anthracene by DMA; fluorescence intensity at 400 nm was plotted against the concentration of DMA. Ideally it should pass through 1 in the ordinate.

Besides collisional quenching, fluorescence quenching can occur by a variety of other processes. Fluorophores can form nonfluorescent complexes with quenchers. This process is referred to as *static quenching* since it occurs in the ground state and does not rely on diffusion or molecular collisions. Static quenching is also described by the Stern-Volmer equation except that the quenching constant is now the association constant (K_{app}). The following figure depicts distinctive features of static and dynamic quenching.

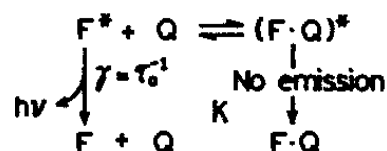


Figure 2-16: Static quenching. F, fluorophore and Q, quencher.

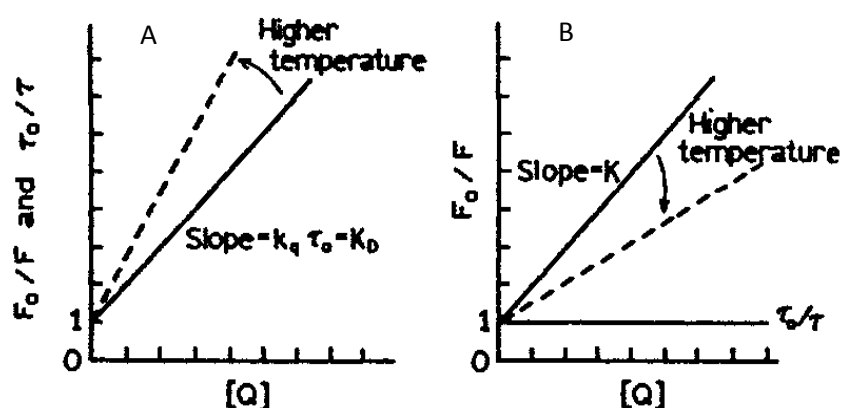


Figure 2-17: Temperature dependencies of static and dynamic quenching. (A) shows the changes in dynamic quenching and (B) in the static quenching with respect to temperature.

Higher temperatures result in faster diffusion and hence larger amounts of collisional quenching. On the contrary, higher temperatures will typically result in the dissociation of weakly bound complexes, and hence smaller amounts of static quenching. For this

reason for dynamic quenching we get high quenching constant with

increasing temperature where as in case of static quenching it decreases. The measurement of fluorescence lifetimes (τ) is the most definitive method to distinguish static and dynamic quenching. For collisional quenching, The decrease in lifetime occurs because quenching is an additional rate process that depopulates the excited state. The decrease in yield occurs because quenching depopulates the excited state without fluorescence emission. Static quenching does not decrease the lifetime because only the fluorescent molecules are observed, and the un-complexed fluorophore have the unquenched lifetime (τ_0). The complexed fluorophore are nonfluorescent, and the only observed fluorescence is from the un-complexed fluorophore. The un-complexed fraction is unperturbed, and hence the lifetime remains the same.

In many instances the fluorophore can be quenched both by collisions and by complex formation with the same quencher. The characteristic feature of the Stern-Volmer plots in such circumstances is an upward curvature, concave toward the y-axis. The Stern-Volmer equation has been modified accordingly,

$$\begin{aligned}
 F_0/F &= (1 + K_S[Q])(1 + K_D[Q]) && \text{where D, donor and A, acceptor} \\
 \text{Or, } F_0/F - 1 &= [K_S + K_D](Q) + K_S K_D [Q]^2 && \text{non-linear } \Delta F/F \text{ vs } [Q] \text{ plot} \\
 \text{Or, } (\Delta F/F) \left(\frac{1}{[Q]} \right) &= [K_S + K_D] + K_S K_D [Q] && \text{linear } K_{app} \text{ vs } [Q] \text{ plot}
 \end{aligned}$$

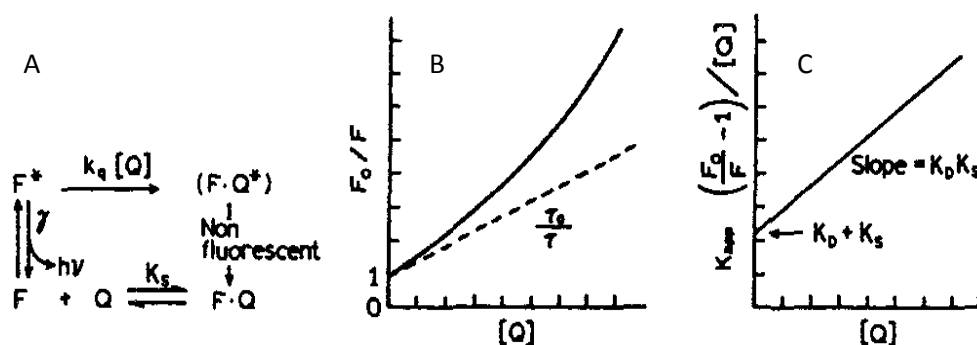


Figure 2-18: Concurrence of static and dynamic quenching (A) is reflected in the upward bending of Stern-Volmer plot (B) whereas the K_{app} vs quencher concentration, $[Q]$, plot (C) shows linearity with a slope of $K_D K_S$ and an intercept of $K_D + K_S$.

Quenching can also occur by a variety of trivial, *i.e.* nonmolecular, mechanisms, such as attenuation of the incident light by the fluorophore itself or other absorbing species.

Another important process that occurs in the excited state is *resonance energy transfer* (RET). This process occurs whenever the emission spectrum of a fluorophore, called the donor, overlaps with the absorption spectrum of another molecule, called the acceptor. The acceptor does not need to be fluorescent. It is important to understand that RET does not involve emission of light by the donor. RET is not the result of emission from the donor being absorbed by the acceptor. Such reabsorption processes (*radiative energy transfer*; vide Appendix) are dependent on the overall concentration of the acceptor, and on non molecular factors such as sample size, and are thus of less interest. There is no intermediate photon in RET (*non-radiative energy transfer*; vide Appendix). The donor and acceptor are coupled by a dipole-dipole interaction. For these reasons, the term RET is preferred to the term fluorescence resonance energy transfer (FRET), which is also in common use. The extent of energy transfer is determined by the distance between the donor and acceptor (*Förster distance*) and the extent of spectral overlap.

Instrumentation

UV-Visible spectrophotometer

It measures the intensity of transmitted light (I) and compares it with the intensity of the incident light (I_0). The ratio I/I_0 is called the transmittance, usually expressed as % T . Absorbance is calculated as follows:

$$A = -\log(\%T/100\%)$$

The basic parts of a spectrophotometer are a light source, a holder for the sample, a diffraction grating or monochromator to separate the different wavelengths of light, and a detector. The radiation source is often a Tungsten filament (300-2500 nm), a deuterium arc lamp (190-400 nm), and more recently light emitting diodes (LED) and Xenon Arc Lamps for the visible wavelengths. The detector is typically a photodiode or a CCD. Photodiodes are used with monochromators, which filter the light so that only light of a single wavelength reaches the detector. Diffraction gratings are used with CCDs, which collect light of different wavelengths on different pixels.

A spectrophotometer can be either single beam or double beam. In a single beam instrument, all of the light passes through the sample cell. I_0 must be measured by removing the sample. This was the earliest design. In a double-beam instrument, the light is split into two beams before it reaches the sample. One beam is used as the reference; the other beam passes through the sample. Some double-beam instruments have two detectors, and the sample and reference beam are measured at the same time. In other instruments, the two beams pass through a beam chopper, which blocks one beam at a time. The detector alternates between measuring the sample beam and the reference beam.

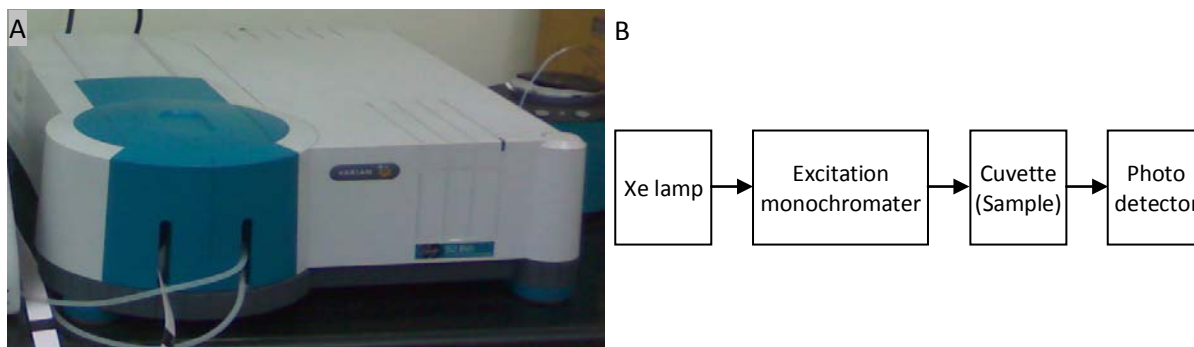


Figure 2-19: (A) Varian Cary 50 absorption spectrophotometers used in our experiments. (B) Block diagram of an absorption spectrophotometer.

Samples for UV-Visible spectrophotometry are most often liquids, although the absorbance of gases and even of solids can also be measured. Samples are typically placed in a transparent cell, known as a cuvette. Cuvettes are typically rectangular in shape, commonly with an internal width of 1 cm. The type of sample container used must allow radiation to pass over the spectral region of interest. The most widely applicable cuvettes are made of high quality fused silica or quartz glass because these are transparent throughout the UV, visible and near infrared regions. Glass and plastic cuvettes are also common, although glass and most plastics absorb in the UV, which limits their usefulness to visible wavelengths.

For our study, *Varian Cary 50* absorption spectrophotometer and 1cm path length quartz cuvettes had been used. *Jasco V-650* had also been used for some experiments.

Spectrofluorimeter

The same mechanism follows here except that the emission monochromator and the photomultiplier are placed at right angle to the beam of excitation light in order to monitor the fluorescence only. And right angle because the rectangular cuvettes are used.

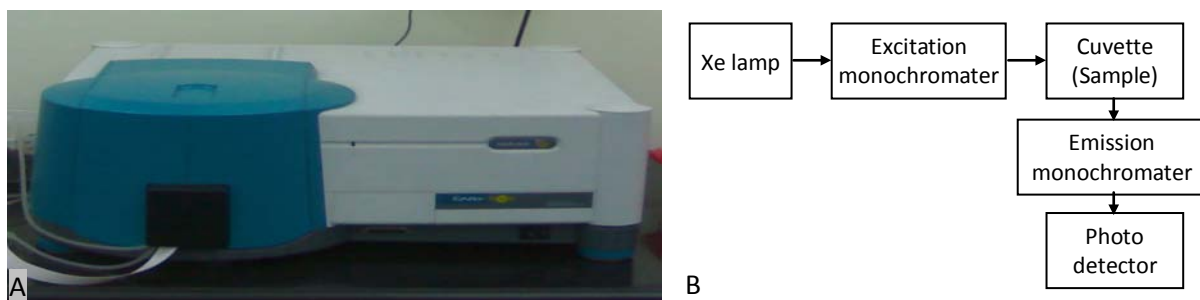


Figure 2-20: (A) Varian Cary Eclipse spectrofluorimeter used in our experiments. (B) Block diagram of a spectrofluorimeter.

For our study, Varian Cary Eclipse spectrofluorimeter and 1cm path length quartz cuvettes had been used. Hitachi F-7000 had also been used for some experiments.

Appendix

Fluorescence Polarization or Anisotropy

Anisotropy measurements are based on the principle of photoselective excitation of fluorophores by polarized light. Fluorophores preferentially absorb photons whose electric vectors are aligned parallel to the transition moment of the fluorophore. The transition moment has a defined orientation with respect to the molecular axes. In an isotropic solution, the fluorophores are oriented randomly. Upon excitation with polarized light, one selectively excites those fluorophore molecules whose absorption transition dipole is parallel to the electric vector of the excitation. This selective excitation results in a partially oriented population of fluorophores (photoselection) and in partially polarized fluorescence emission. Emission also occurs with the light polarized along a fixed axis in the fluorophore. The relative angle between these moments determines the maximum measured anisotropy. The fluorescence anisotropy (r) and polarization (P) are defined by

$$r = \frac{I_{\parallel} - I_{\perp}}{I_{\parallel} - 2I_{\perp}} \quad \& \quad P = \frac{I_{\parallel} - I_{\perp}}{I_{\parallel} + I_{\perp}}$$

Where I_{\parallel} and I_{\perp} are the fluorescence intensities of the vertically (\parallel) and horizontally (\perp) polarized emission, when the sample is excited with vertically polarized light. Anisotropy and polarization are both expressions for the same phenomenon, and these values are interconvertible.

Several phenomena can decrease the measured anisotropy to values lower than the maximum theoretical values. The most common cause is rotational diffusion. Such diffusion occurs during the lifetime of the excited state and displaces the emission dipole of the fluorophore. Transfer of excitation between fluorophores also results in decreased anisotropies.

Solvent relaxation

The length of time fluorescent molecules remain in the excited state provides an opportunity for interactions with other molecules in solution. One example of such dynamic processes in solution involve fluorophore-solvent interactions and rotational diffusion. As was observed by Stokes, most fluorophores display emission at lower energies than their absorption. Most fluorophores have larger dipole moments in the excited state than in the ground state. Rotational motions of small solvent molecules in fluid solution are rapid, typically occurring on a timescale of 40 *picoseconds* or less. The relatively long timescale of fluorescence (in nanosecond order) allows ample time for the solvent molecules to reorient around the excited-state dipole, which lowers its energy and shifts the emission to longer wavelengths. This process is called solvent relaxation and occurs in 10^{-10} s in fluid solution. It is these differences between absorption and emission that result in the high sensitivity of emission spectra to solvent polarity, and the smaller spectral changes seen in absorption spectra. Solvent relaxation can result in substantial Stokes' shifts.

Radiative energy transfer

Radiative energy transfer or the *inner filter effect* is the result of emission from the donor being absorbed by the acceptor. When the acceptor and the donor are the part of a same molecule (*viz.* tryptophan and heme in met-myoglobin), it results in a phenomenon called *self quenching*.

In fluorescence quenching experiments, if the sample shows any significant absorbance (more than 0.05 O.D.) either at the excitation wavelength or at the emission maxima, observed fluorescence intensity should be *corrected* using the following formula

$$F_{corr} = F_{obs} \cdot \text{antilog} \left(\frac{OD_{ex} + OD_{em}}{2} \right)$$

Non-radiative energy transfer

As discussed earlier the mechanism does not involve any mediation of photon. Dipole-dipole interaction between donor and acceptor may lead to resonance (Coulomb) energy transfer; the electron transfer (exchange energy transfer) may also take place producing excited state species that can be detected by *laser flash photolysis* experiments.

The Figure 2-21,22 shows plausible explanation of resonance energy transfer. When an excited state electron of the donor drops down from the LUMO to the HOMO, it induces the transition of a ground state electron of the acceptor to the excited state. Extent of energy transfer depends on the degree of spectral overlap and the donor acceptor distance (*Förster distance*) given by the following equation

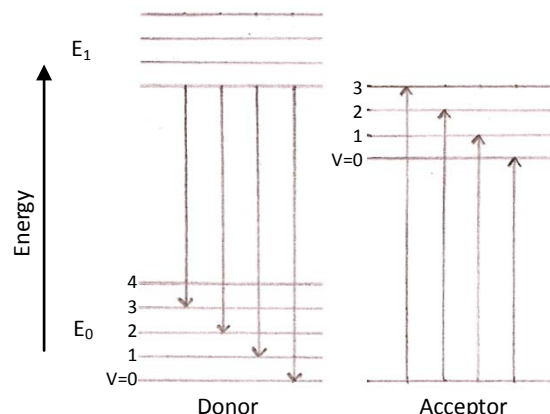


Figure 2-21: Resonance energy transfer.

$$P = \frac{F_D \int \epsilon_A}{R_{DA}^6}$$

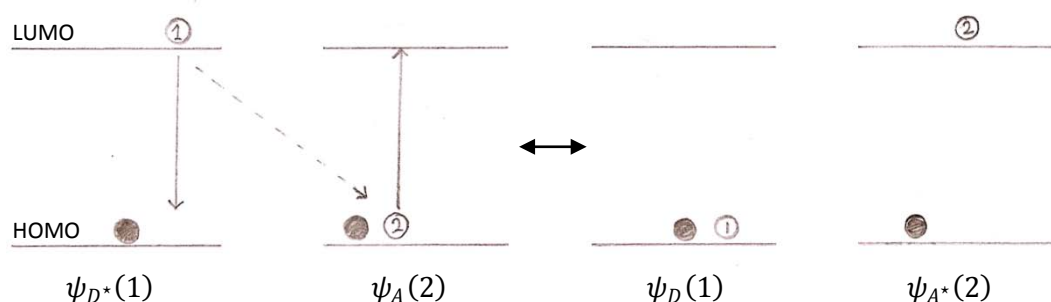


Figure 2-22: When an excited state electron of the donor drops down from the LUMO to the HOMO, it induces the transition of a ground state electron of the acceptor to the excited state. D, Donor and A, acceptor; ○, is the electron undergoing transition and the filled circle represents the ground state electron.

Where the subscripts D and A denote donor and acceptor respectively, P is the extent of energy transfer, and R is the Förster distance. In quantum mechanical terms it can be expressed by the overlap integral, $\langle \psi_{D^*}(1) \psi_A(2) | \psi_D(1) \psi_{A^*}(2) \rangle$.

On the contrary, the exchange energy transfer (Figure: 2-23) is given by the following overlap integral, $\langle \psi_{D^*}(1) \psi_A(2) | \psi_D(2) \psi_{A^*}(1) \rangle$. The extent of energy transfer varies exponentially with the donor acceptor distance ($P \propto e^{-R}$).

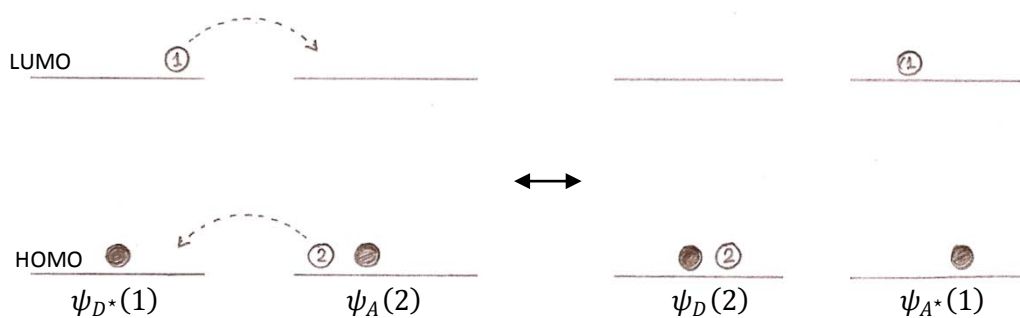


Figure 2-24: Exchange energy transfer showing the exchange of electron between donor and acceptor. D, Donor and A, acceptor; ○, is the electron undergoing transition and the filled circle represents the ground state electron.

Raman scatter

The Figure 2-25 shows the emission spectrum of a dilute solution of spectrin (0.05 μM) in aqueous buffer. The broad peak at 340 nm is the tryptophan fluorescence, and the small sharp peak at ~ 320 nm is the Raman scatter. For water, this peak appears at 3600-cm^{-1} lower wavenumber than the exciting light. For excitation at 295 nm, the Raman peak from water occurs at ~ 326 nm. For highly fluorescent samples, the emission spectrum generally

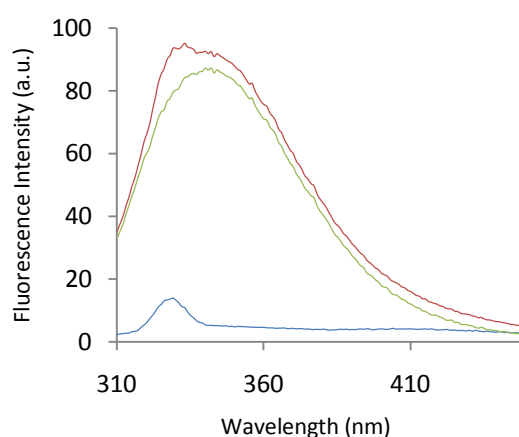


Figure 2-25: Shows the tryptophan fluorescence emission spectrum of spectrin (0.05 μM) as obtained (red line). The buffer blank shows the Raman scatter (blue line). The green line is the corrected emission spectrum of spectrin. $\lambda_{\text{ex}} = 295$ nm.

overwhelms the Raman peak. However, if the gain of the instrument is increased to compensate for a dilute solution or a low quantum yield, the Raman scatter may become significant and distort the emission spectrum.

Since Raman scatter always occurs at a constant wavenumber difference from the incident light, such scatter can be identified by changing the excitation wavelength.

References

- S.R. Palit, **Elementary Physical Chemistry**, 1997, 30ed:95-97.
 - J.R. Lakowicz, **Principles of Fluorescence Spectroscopy**, 2ed.
 - D. Freifelder, **Physical Biochemistry: Application to Biochemistry and Molecular Biology**, 2ed:494-572.
 - **Wikipedia**, <http://en.wikipedia.org/wiki/>
 - Molecular Expressions, **Optical Microscopy Primer: Basic Concepts in Fluorescence**, <http://micro.magnet.fsu.edu/primer/techniques/fluorescence/fluorescenceintro.html>
 - Jobin Yvon, Horiba Scientific, **A Guide to Recording Fluorescence Quantum Yields**, <http://www.horiba.com/us/en/scientific/products/fluorescence-spectroscopy/application-notes/quantum-yields/>
-
- [1] I. Fitos, J. Visy, F. Zsila, G. Mády, M. Simonyi, **Selective binding of imatinib to the genetic variants of human α_1 -acid glycoprotein**, *Biochimica et Biophysica Acta* 2006, 1760:1704–1712.
 - [2] S.K. Nayaki, M. Swaminathan, **Unusual luminescence characteristics of aminobiphenyls**, *Spectrochim, Acta, Part A: Mol. Biomol. Spectrosc.* 2002, 58:2931–2940.
 - [3] S.K. Nayaki, M. Swaminathan, **Spectral characteristics of 2-aminodiphenylamine in different solvents and at various pH values**, *Spectrochim, Acta, Part A: Mol. Biomol. Spectrosc.* 2001, 57:1361–1367.
 - [4] P. Jana, T. Ganguly, S.K. Sarkar, A. Mitra, P.K. Mallick, **N heteroatomic effect on the photophysics of a polyphenyl system: 2,2'-dipyridylamine**, *J. Photochem. Photobiol., A Chem.* 1996, 94:113–118.
 - [5] F.D. Lewis, T.M. Long, C.L. Stern, W. Liu, **Structures and excited states of extended and folded mono-, di-, and tri-N-arylbenzamides**, *J. Phys. Chem., A* 2003, 107: 3254–3262.
 - [6] J.T. Edward, H.S. Chang, K. Yates, R. Stewart, **Protonation of the amide group. I. The basicities of substituted benzamides**, *Can. J. Chem.* 1960, 38:1518–1525.
 - [7] S.K. Nayaki, M. Swaminathan, **Excited state solvatochromic and prototropic behaviour of 4-aminodiphenylamine and 4,4'-diaminodiphenylamine—A comparative study by electronic spectra**, *Spectrochim. Acta, Part A: Mol. Biomol. Spectrosc.* 2006, 64:631–636.

off the track

Understanding CD Spectroscopy

with Professor Pradeep Kumar Sengupta

Biophysics Division

Saha Institute of Nuclear Physics, Kolkata

Circular Dichroism (CD) is the differential absorption of left- and right-handed circularly polarized light. CD was discovered by the French physicist Aimé Cotton in 1896.

A CD Spectrometer is an instrument that records this phenomenon as a function of wavelength. This phenomenon is exhibited in the absorption bands of an optically active molecule. Because a large fraction of biological molecules contain optically active centers, CD has great applicability to their study. CD can be used to help determine the structure of macromolecules (including the secondary structure of proteins and the handedness of DNA). However, the theory concerning the spectra with molecular structure is not yet fully developed. Thus, the working rules used to interpret spectra are for the most part empirical.

Circularly polarized light

Linearly polarized light is polarized in a certain direction *i.e.* the magnitude of its electric field vector oscillates only in one plane, similar to a sine wave (Figure 3-1). In circularly polarized light, the electric field vector has a constant length, but rotates about its propagation direction. Hence, it forms a helix in space while propagating (Figure 3-2A). If this is a left-handed helix, the light is referred to as left circularly polarized, and vice versa for a right-handed helix.

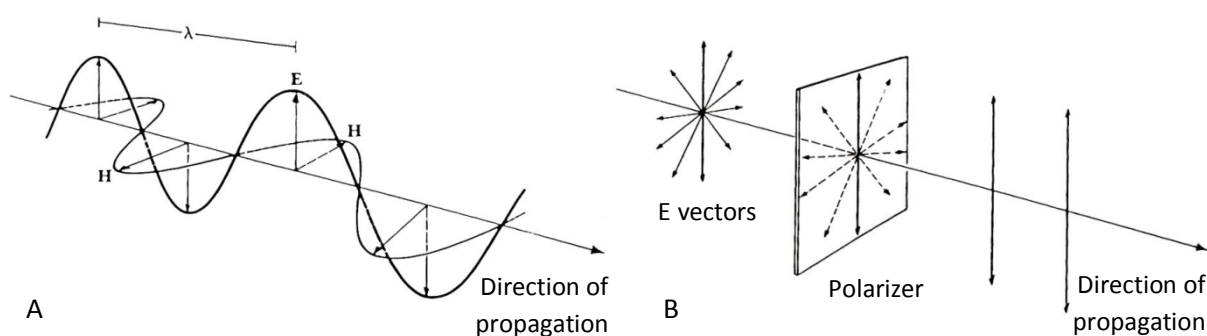


Figure 3-1: (A) Propagation of an electromagnetic wave. The E and H vectors and the direction of propagation are mutually perpendicular. The plane of the E vector is called the plane of polarization. (B) Production of plane-polarized light. A collection of waves falls on the polarizer, which passes only those components of the E vector that are parallel to the axis of the polarizer.

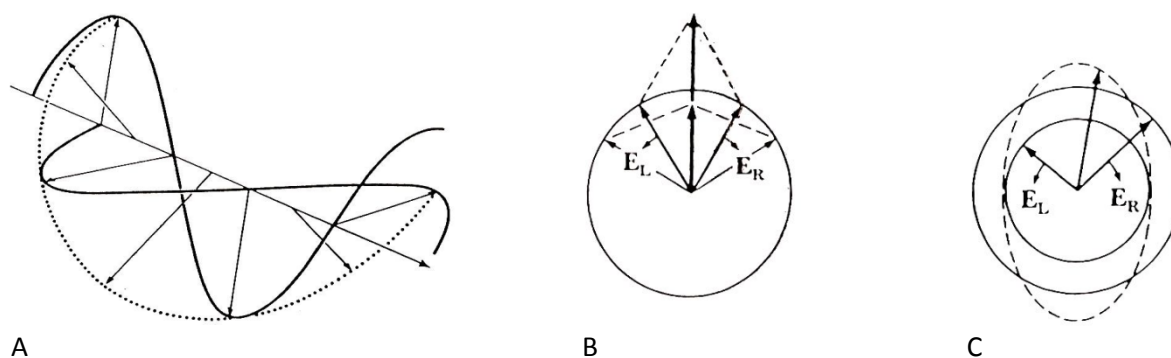


Figure 3-2: (A) Generation of circularly polarized light. The E vectors of two electromagnetic waves are one-quarter wavelength out of phase and are perpendicular. The vector that is the sum of the E vectors of the two components rotates so that its tip follows a helical path (dotted line). (B) & (C) shows how right and left circularly polarized light combine. If the two waves have the same amplitude, the result is plane polarized light (B); and if their amplitudes differ, the result is elliptically polarized light (C) *i.e.* the head of the resultant vector will trace the ellipse shown as a dashed line. The ellipticity, $\theta = \tan^{-1} b/a$ where a and b are the major and minor axes of the ellipse.

Suppose that two plane-polarized waves differing in phase by one quarter wavelength, whose E vectors are perpendicular to one another, are superimposed. As the waves propagate forward, the resultant E vector rotates so that its tip follows a helical path (Figure 3-2A). This is also true for the magnetic field vector. If a right and left circularly polarized wave, both of equal amplitude, are superimposed, the resultant is plane polarized light, because at any point in space the E vector or each will sum as shown in Figure 3-2B. *Similarly the plane-polarized light can be decomposed into left and right components.* If the amplitudes of the two circularly polarized waves are not the same, the tip of the resultant E vector will follow an elliptical path and such light is said to be elliptically polarized. A parameter called the ellipticity, θ , is often used to describe the elliptical polarization. This is the angle whose tangent is the ratio of the minor and major axes of the ellipse shown in Figure 3-2C.

Optical Activity and Circular Dichroism

The behavior of some molecules is sensitive to the plane of polarization of the incident light. Such a molecule or chromophore is called optically active and is characterized by having distinct molar absorption coefficients, ε_L and ε_R , for left and right circularly polarized lights, respectively. Optical activity is a characteristic of many organic and almost all biological molecules. The property that determines whether a chromophore is optically active is its asymmetry. If a molecule is asymmetric in the sense that it cannot be superimposed on its mirror image, it is optically active.

As indicated earlier, a plane polarized wave can be thought of as a mixture of left and right circularly polarized light. Therefore, if a substance retards both left and right equally, the left and right waves will recombine on leaving the substance to form plane-polarized light, with the plane of the transmitted beam being the same as that of the incident beam. However, if the retardation is unequal, on leaving the material the E vectors of the left and right waves combine to form a beam of plane polarized light whose angle differs from that of the plane of polarization of the incident wave; hence, the plane of polarization of the resulting wave will be rotated. This difference is usually expressed in terms of the absorption coefficients for left and right circularly polarized light:

$$\varepsilon_L - \varepsilon_R = \Delta\varepsilon$$

In which $\Delta\varepsilon$ is called the circular dichroism, or CD. It is positive if $\varepsilon_L - \varepsilon_R > 0$ and negative if $\varepsilon_L - \varepsilon_R < 0$. Experimentally, it is usual to measure $\Delta\varepsilon$, but for historical reasons the ellipticity, θ , is plotted. θ is defined as

$$\theta = 2.303(A_L - A_R) \cdot 180 / 4\pi = 33 \Delta A \text{ degrees}$$

In which A is the absorbance. A curve showing the dependence of θ on wavelength is called a CD curve or CD spectrum. An important point is that, *if a given optically active molecule has positive CD, its mirror image will have a negative CD of precisely the same magnitude.*

Cotton effect

The Cotton effect is the characteristic change in optical rotatory dispersion and/or circular dichroism in the vicinity of an absorption band of a substance. In a wavelength region where the light is absorbed, the absolute magnitude of the optical rotation at first varies rapidly with wavelength, crosses zero at absorption maxima

and then again varies rapidly with wavelength but in opposite direction. This phenomenon was discovered in 1895 by the French physicist Aimé Cotton (1869-1951).

The Cotton effect is called positive if the optical rotation first increases as the wavelength decreases (as first observed by Cotton), and negative if the rotation first decreases. Protein structure like beta sheet shows positive Cotton Effect. These curves are only rarely studied now. For proteins and polypeptides the principal Cotton effect occurs in the wavelength range near 200 nm and is caused by the absorption of the peptide bond. For nucleic acids, it occurs in the 250-275 nm range and is caused by electronic transitions of the nucleotide bases. A positive CD band always corresponds to a positive Cotton effect.

Results and Discussion

Peptide bond which is the principal element whose spectrum is detected by CD, exists in many conformations depending on its precise location in the protein, the spectrum is a result of an average of the various conformation parameters. Hence, in practice, an empirical approach of obtaining an CD spectrum for molecules whose structure is accurately known from X-ray diffraction is used, and the spectrum is related to the structural features of the molecule. This spectrum is then compared with the spectrum of a protein of unknown structure. In such an approach, it is assumed that the structure of a macromolecule in solution (CD is determined in solution) is nearly the same as that of a fibre, crystal, or dry powder (as is used in X ray analysis) prepared from the same solvent.

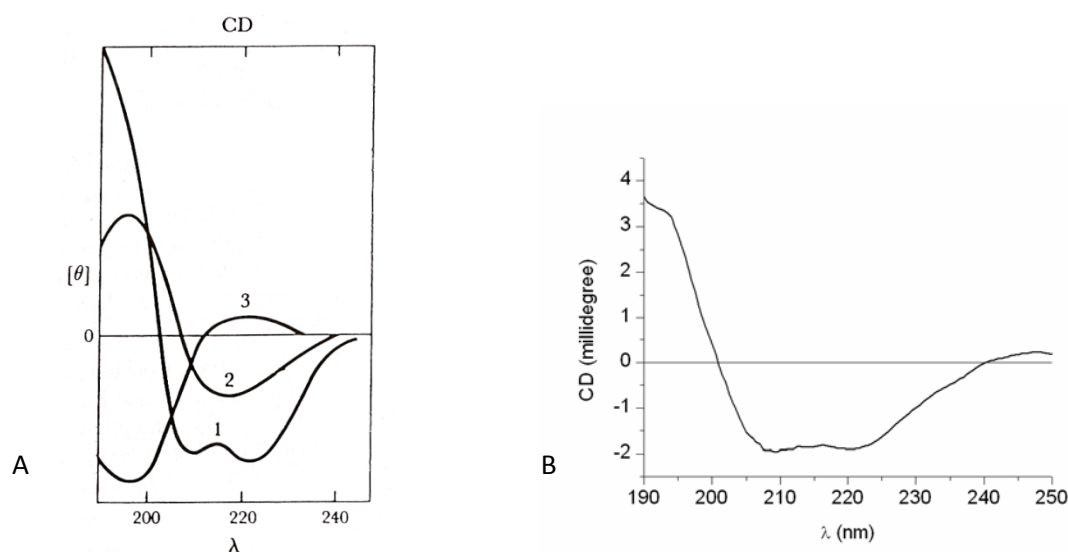


Figure 3-3: (A) CD spectra for poly-L-lysine in the α -helical (1), β (2), and random-coil (3) conformations. **(B)** Observed CD curve for ovine erythroid spectrin (1.5 μ M) in 10 mM phosphate buffer, 50 mM KCl, obtained in MOS-450 Spectrometer using 0.1 mm pathlength cuvette.

The CD spectrum for ovine erythroid spectrin (Figure 3-3B) suggested spectrin to be an α -helix major protein when compared with the standard CD spectra for poly-L-lysine in different conformations (Figure 3-3A).

CD is extraordinarily sensitive to changes in conformation—if a CD spectrum changes in any way, there must be a conformational change. Hence, even if the structure is not known at all and the CD curve is virtually uninterpretable, CD analysis can still be a sensitive assay for any interaction or agent that causes a conformational change.

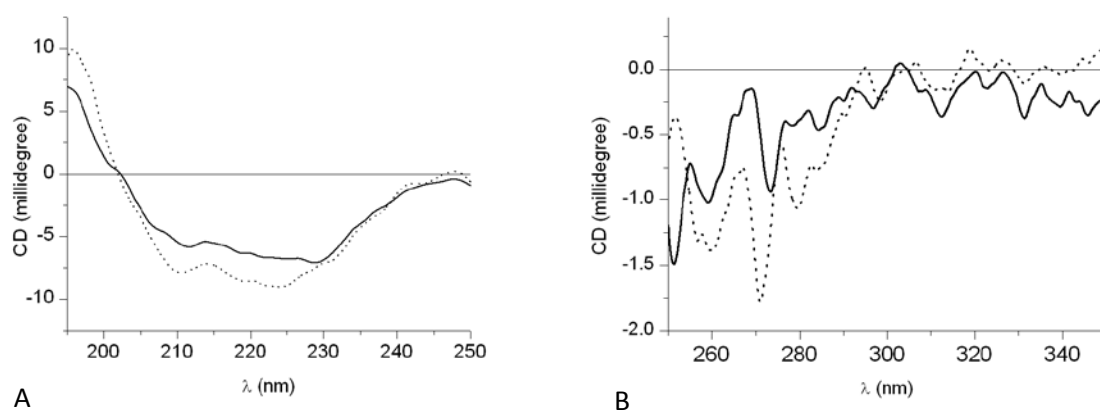


Figure 3-4: (A) Far-UV CD for ovine erythroid spectrin (1 μ M in 10 mM phosphate buffer, 50 mM KCl) alone (solid line) and in presence of 60 μ M menadione in acetonitrile solvent. (B) Near-UV CD for ovine erythroid spectrin (1 μ M in 10 mM phosphate buffer, 50 mM KCl) alone (solid line) and in presence of 30 μ M imatinib in DMSO. The spectra were obtained in Jasco-720 Spectropolarimeter; near-UV spectra were obtained using 10 mm pathlength rectangular cuvette and the far-UV spectra using 1 mm pathlength cylindrical cuvette.

Figure 3-4A shows the representative far-UV CD spectra of spectrin in presence and in the absence of the drug, menadione. It shows a significant change in the characteristic α -helical structure of spectrin upon association with menadione indicating alteration in the polypeptide backbone of the protein. The near-UV spectra shown in the Figure 3-4B indicated significant change in the shape and intensity upon binding to imatinib. The results from near-UV regions indicate that there is a change in the tertiary structure of the protein upon binding of imatinib.

Whether the ligand receptor interactions are reversible can also be demonstrated with CD spectroscopy. Restoration of the CD signal to that of receptor alone, after dialyzing the ligand receptor mixture indicates reversible binding.

Induced CD: An optically inactive ligand when binds its receptor a chirality may be induced to the ligand, which can be demonstrated in the CD signal. Therefore, study of induced CD may be a potential tool to monitor some ligand protein interaction.

References

- D. Freifelder, **Optical Rotatory Dispersion and Circular Dichroism**, Physical Biochemistry: Application to Biochemistry and Molecular Biology, 2ed:572-602.
- **Wikipedia**, <http://en.wikipedia.org/wiki/>
- **Animated Electromagnetic Waves**, <http://www.enzim.hu/~szia/cddemo/edemo1.htm>
- **Circular Dichroism**, http://www.ap-lab.com/circular_dichroism.htm
- **An Introduction to Circular Dichroism**, <http://www.photophysics.com/circulardichroism.php>
- L. Whitmore, B.A. Wallace, **Protein secondary structure analyses from circular dichroism spectroscopy: methods and reference databases**, Biopolymers 2008, 89(5):392–400.
- N.J. Greenfield, **Using circular dichroism spectra to estimate protein secondary structure**, Nature protocols 2006, 1(6):2876–2890.
- G.D. Fasman, **Circular Dichroism and the Conformational Analysis of Biomolecules** (1996) Plenum Press, New York; available at Google books, <http://books.google.co.in/>

“He who makes two blades of grass grow where one grew before is the benefactor of mankind; but he who obscurely worked to find the laws of such growth is the intellectual superior as well as the greater benefactor of the two.”

—Rowland, 1899

The End